[66] —, "Toward a unified theory of modulation," *Proc. IEEE*, vol. 54, pp. 340–353, Mar. 1966, and pp. 735–755, May 1966.
[67] —, "Generation of digital signalling waveforms," *IEEE Trans. Commun.*, vol. COM-16, pp. 81–93, Feb. 1968.
[68] —, "Method and apparatus for intepolation and conversion of signals specified by real and complex zeros," U.S. Patent 3510640, May 1970.
[69] —, "Zero-crossing properties of angle-modulated signals," *IEEE Trans. Commun.*, vol. COM-20, pp. 307–315, June 1972.
[70] H. B. Voelcker and A. A. G. Requicha, "Clipping and signal determinism: Two algorithms requiring validation," *IEEE Trans. Commun.*, vol. COM-21, pp. 738–744, June 1973.
[71] —, "Band-limited random-real-zero signals," *IEEE Trans. Commun.*, vol. COM-21, pp. 933–936, Aug. 1973.
[72] A. Walther, "The question of phase retrieval in optics," *Opt. Acta*, vol. 10, pp. 41–49, Jan. 1963.
[73] N. Wiener, *The Fourier Integral and Certain of its Applications*. New York: Dover, 1958.
[74] E. Wolf, "Is a complete determination of the energy spectrum of light possible from measurements of the degree of coherence?" *Proc. Phys. Soc.*, vol. 80, part 6, pp. 1269–1272, 1962.
[75] J. L. Yen, "On nonuniform sampling of bandwidth-limited signals," *IRE Trans. Circuit Theory*, vol. CT-3, pp. 251–257, Dec. 1956.
[76] M. Zakai, "Band-limited functions and the sampling theorem," *Inform. Contr.*, vol. 8, pp. 143–158, 1965.
[77] A. Zygmund, *Trigonometric Interpolation*. Chicago, IL: Univ. of Chicago Press, 1950.

Introduction to Spread-Spectrum Antimultipath Techniques and Their Application to Urban Digital Radio

GEORGE L. TURIN, FELLOW, IEEE

Abstract—**In a combination tutorial and research paper, spread-spectrum techniques for combating the effects of multipath on high-rate data transmissions via radio are explored. The tutorial aspect of the paper presents: 1) a heuristic outline of the theory of spread-spectrum antimultipath radio receivers and 2) a summary of a statistical model of urban/suburban multipath. The research section of the paper presents results of analyses and simulations of various candidate receivers indicated by the theory, as they perform through urban/suburban multipath. A major result shows that megabit-per-second rates through urban multipath (which typically lasts up to 5 μs) are quite feasible.**

I. Introduction

SOME DIGITAL radio systems must operate through an extremely harsh multipath environment, in which the duration of the multipath may exceed the symbol length.[1] Two disciplines combine to shed light on receiver design for this environment: the modeling and simulation of multipath channels and the theory of multipath and other diversity receivers.

In this paper, we first present a tutorial review of pertinent aspects of both underlying disciplines, particularly in the context of spread-spectrum[2] systems. We then carry out rough analyses of the performances of two promising binary spread-spectrum antimultipath systems. Finally, since the analyses contain a number of oversimplifications that make them heuristic rather than definitive, we present results of computer simulations of the two proposed configurations and others, as they operate through simulated urban/suburban multipath. The simulation results highlight the importance of using realistic simulations of complex channels rather than simplified analyses, or they show that the analytic results, although based on standard assumptions, are unduly optimistic.

II. Modeling Multipath Propagation

Ultimately, a reliable multipath model must be based on empirical data rather than on mathematical axioms. Two types

Manuscript received February 8, 1979; revised October 9, 1979. This work was supported by the National Science Foundation under Grant ENG 21512 and SRI International under Advanced Research Projects Agency Contract MDA 903-78-C-0216.

The author is with the Department of Electrical Engineering and Computer Sciences and the Electronics Research Laboratory, University of California, Berkeley, CA 94720.

[1] An example is the ARPA Packet Radio network [38].

[2] In a spread-spectrum system, the bandwidth W of the transmitted signals is much larger than $1/T$, the reciprocal of the duration of the fundamental signalling interval, so $TW >> 1$. The transmitted spectrum is said to be "spread" since a signal lasting T seconds need not occupy more than the order of $W \cong 1/T$ Hz of bandwidth, in which case $TW \cong 1$. See [6] for references on the spread-spectrum concept.

0018-9219/80/0300-0328$00.75

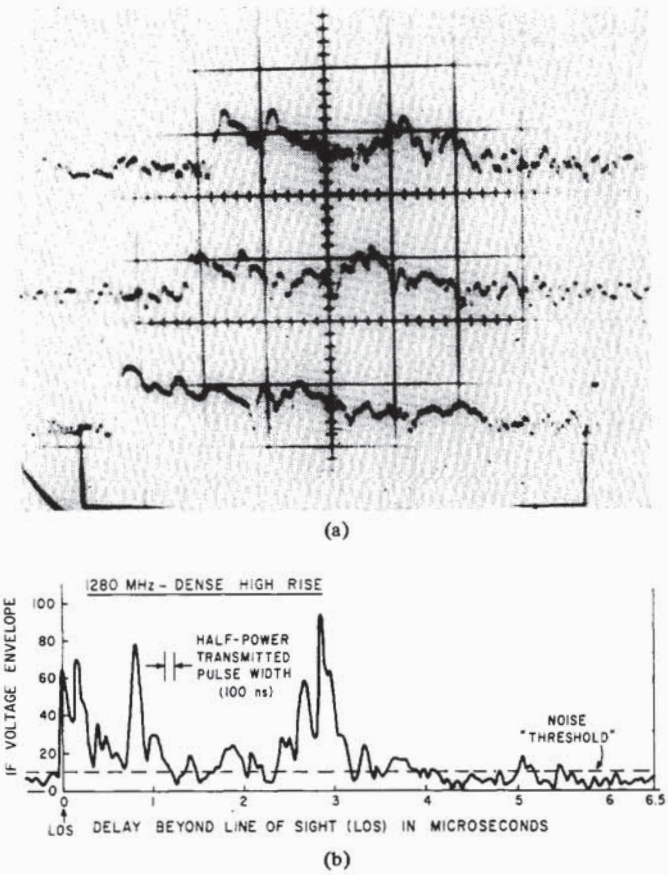

Fig. 1. Example of measured multipath profiles for a dense high-rise topography. (a) Top to bottom: 2920, 1280, 488 MHz. Vertical scale: 35 dB/cm. Horizontal scale: 1 μs/cm. Different apparent LOS delays are due to difference in equipment delays. (b) Middle trace of (a) on a linear scale.

of data are available. The more common type give the results of narrow-band or CW measurements, in which only a single fluctuating variable, a resultant signal strength, is measured [11]. Although the fluctuation of this strength variable depends on reception via multiple paths, these paths are not resolved by the measurements. We shall denote the results of such measurements as "fading" data rather than multipath data, because they determine a fading distribution of the single strength variable, e.g., Rayleigh, log-normal, Rice, etc.

Wide-band experimental data that characterize individual paths are less common [5], [10], [19], [33], [37]. In order to resolve two paths in such measurements, the sounding signal's bandwidth must be larger than the reciprocal of the difference between the paths' delays. Although bandwidths of 100 MHz or more have been used in exceptional circumstances to resolve path delay differences of less than 10 ns [10], the bulk of available data derives from 10-MHz bandwidths or less [5], [19], [33], [37]. In the latter measurements, paths separated by delays of more than 100 ns are resolved; multiple paths with smaller separations are seen as single paths.

The nature of the multipath measurements depends somewhat on the use envisioned for them. If understanding of the effect of the multipath channel on CW transmissions is required, measurements that show Doppler effects may be important [5], and these are reasonably related to a scattering-medium model of the channel [1], [12]. For high-rate packetized-data transmission, for vehicle-location sensing, and for other "bursty" transmissions, measurement of sequences of "impulse responses" of the propagation medium suffices.

The simulations of data reception that are presented in a later section are based on the "impulse response" approach, and it is to this type of model that we restrict ourselves. In order that the model and the simulations themselves be fully understood, we shall review here the experiments underlying the model. These were performed in urban/suburban areas [32], [33].

A. The Underlying Experiments

Pulse transmitters were placed at fixed, elevated sites in the San Francisco Bay Area. Once per second, these would simultaneously send out 100-ns pulses of carrier at 488, 1280, and 2920 MHz. The pulses were received in a mobile van that moved through typical urban/suburban areas, recording on a multitrace oscilloscope the logarithmically scaled output of the receiver's envelope detectors (see Fig. 1). Since the oscilloscope was triggered by a rubidium frequency standard that was synchronized with a similar unit at the transmitters prior to each experimental run, absolute propagation delays could be measured within experimental accuracies of better than 20 ns.

Four series of experiments were performed, in the following typical urban/suburban areas:

A) dense high-rise–San Francisco financial district,
B) sparse high-rise–downtown Oakland,
C) low rise–downtown Berkeley,
D) suburban–residential Berkeley.

In each area, regions of dimensions roughly 500–1000 ft (along the transmitter–receiver line of sight) by 2500–4000 ft (tangential to line of sight) were exhaustively canvassed, with care taken to include proper topographic cross sections: intersections, midblocks, points at which the transmitter site was visible or occluded, etc. About 1000 frames of data of the type shown in Fig. 1(a) were obtained in each area.

B. A Fundamental Model

The model upon which data reduction was based was one first posed in [27]. In this model, it is assumed that a transmission of the form

$$s(t) = \mathrm{Re}\,[\sigma(t)\exp(j\omega_0 t)] \tag{1}$$

will be received as

$$r(t) = \mathrm{Re}\,[\rho(t)\exp(j\omega_0 t)] + n(t) \tag{2}$$

where

$$\rho(t) = \sum_{k=0}^{K-1} a_k\,\sigma(t - t_k)\exp(j\theta_k). \tag{3}$$

In (1)–(3), $\sigma(t)$ is the complex envelope of the transmission, i.e., $|\sigma(t)|$ is its amplitude modulation and $\tan^{-1}[\mathrm{Im}\,\sigma(t)/\mathrm{Re}\,\sigma(t)]$ is its phase modulation. The transmission is received via K paths, where K is a random number that may vary from transmission to transmission. The kth path is characterized by three variables: its strength a_k, its modulation delay t_k, and its carrier phase shift θ_k. The waveform $n(t)$ is an additive noise component.

In the context of the spread-spectrum systems on which we shall concentrate, it is desirable to assume that all paths are

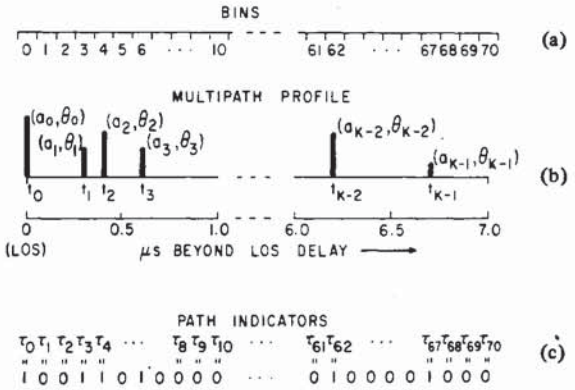

Fig. 2. Discrete-time model. (a) Division of excess delay axis into seventy one 100-ns bins. (b) A typical multipath profile. (c) Discrete-time path-delay indicator string, $\{\tau_l\}_{l=0}^{70}$.

resolvable, i.e., that

$$|t_k - t_l| > 1/W, \qquad \text{for all } k \neq l \tag{4}$$

holds, where W is the transmission bandwidth. Distinct paths in the physical medium that violate this resolvability condition are not counted separately, since they cannot be distinguished by a measurement using bandwidth W. Instead, any two paths—call them k_1 and k_2—for which $|t_{k_1} - t_{k_2}| < 1/W$ are considered as a single path in (3), with a common delay $t_k \cong t_{k_1} \cong t_{k_2}$ and a strength/phase combination given by

$$a_k \exp(j\theta_k) \triangleq a_{k_1} \exp(j\theta_{k_1}) + a_{k_2} \exp(j\theta_{k_2}).$$

It is the triplet $\{t_k, a_k, \theta_k\}$ that is to be determined for each "resolvable" path. To be sure, if a continuum of paths existed, it would be difficult uniquely to cluster the "subpaths" into paths. But many media, including the urban/suburban one, have a natural clustering, e.g., groups of facades on buildings, that make the model feasible.

C. A Discrete-Time Approximation to the Model

In addition to the additive random noise $n(t)$ in (2), the received signal $r(t)$ is therefore characterized by the random variables $\{t_k\}_0^{K-1}$, $\{a_k\}_0^{K-1}$, $\{\theta_k\}_0^{K-1}$ and K. The purpose of data reduction from the "multipath profiles" exemplified by Fig. 1 was to obtain statistics of these random variables upon which to base a simulation program. A number of generations of statistical models—based both on the data and on physical reasoning when the data were insufficient or undecisive—ensued [8], [9], [25], [26], [32]. The following final version emerged.

Each multipath profile starts with the line-of-sight (LOS) delay, which is chosen as the delay origin. Since the resolution of the original experiment is 100 ns, the delay axis is made discrete by dividing it into 100-ns bins, numbered from 0 to 70. Bin 0 is centered on LOS delay, subsequent bins being centered on multiples of 100 ns. The delay of any physical path lying in bin l is quantized to $100l$ ns, the delay of the bin's center. Fig. 2 shows the bin structure, a multipath profile, and the resulting discrete-time path-delay structure. Notice that only paths with delays less than 7.05 μs beyond LOS delay are encompassed in this model; experimental evidence shows that significant paths with larger delays are highly improbable.

The path-delay sequence $\{t_k\}_0^{K-1}$ is approximated by a string $\{\tau_l\}_0^{70}$ of 0's and 1's, as shown in Fig. 2(c). If a path exists in bin l, $\tau_l = 1$; otherwise $\tau_l = 0$. In the sample string in Fig. 2(c), only $\tau_0, \tau_3, \tau_4, \tau_6, \cdots, \tau_{62}, \tau_{67}$ are nonzero, corresponding to the quantized path delays $\tilde{t}_0 = 0$, $\tilde{t}_1 = 300$ ns, $\tilde{t}_2 = 400$ ns, $\tilde{t}_3 = 600$ ns, $\cdots$, $\tilde{t}_{K-2} = 6200$ ns, $\tilde{t}_{K-1} = 6700$ ns. ($\tilde{t}_k$ is the value of t_k, as quantized to the nearest 100 ns.)

Associated with each nonzero τ_l is the corresponding (a_k, θ_k) pair. Thus the discrete-time model is completed by appending to the τ_l string a set of strength-phase pairs $\{(a_k, \theta_k)\}_{k=0}^{K-1}$, where the index k refers to the kth nonzero entry in the τ_l string. This is shown in Fig. 2(b).

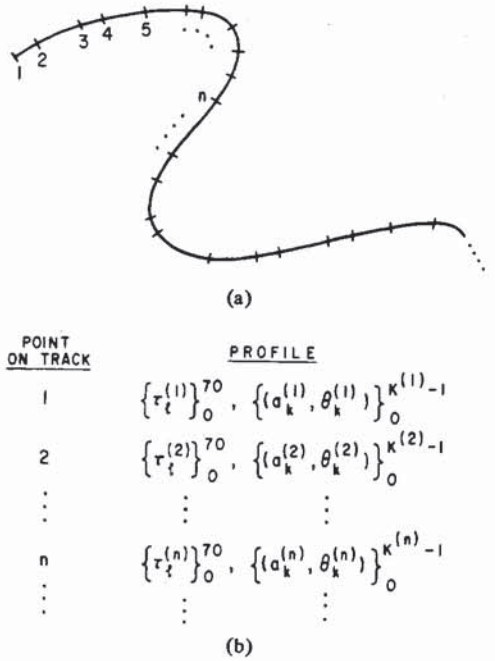

Fig. 3. Spatial variation of the multipath profile. (a) A vehicle's track, with spatial sample points. (b) The sequence of multipath profiles at the sample points on the track.

The discrete-time model of Fig. 2 pictures the multipath profile at a single point in space. A *sequence* of such profiles is needed to depict the progression of multipath responses that would be encountered by a vehicle following a track such as shown in Fig. 3(a). One imagines points $1, 2, \cdots, n, \cdots$, arbitrarily placed on the track, at each of which a multipath response is seen. The discrete-time versions of these responses are arrayed in Fig. 3(b), where an additional spatial index n has been superscribed on all variables.

One begins to recognize the complexity of the model and of the required reduction of experimental data on realizing that in addition to the need for first-order statistics of the random variables $\tau_l^{(n)}$, $a_k^{(n)}$, $\theta_k^{(n)}$, and $K^{(n)}$ (where $0 \leqslant l \leqslant 70$; $0 \leqslant k \leqslant K^{(n)} - 1$; $1 \leqslant n < \infty$), there are two dimensions along which at least second-order statistics are necessary: temporal and spatial. For each profile (fixed n), there are temporal correlations of the delays, strengths and phases of the several paths; in addition, there are spatial correlations of these variables at neighboring geographical points.

The reduction of experimental data [9], [25], [33] and physical reasoning led to the following model, which was the basis for simulation.

1) The $\{\tau_l^{(n)}\}$ string of the nth profile is a modified Bernoulli sequence, in which the probability of a 1 in the lth place depends on: a) the value of l; b) whether a 1 or a 0 occurred in the $(l-1)$th place of the same profile; c) whether a 1 or a 0 occurred in the lth place of the $(n-1)$th profile.

2) The strength $a_k^{(n)}$ of the kth path of the nth profile is conditionally log-normally distributed,[3] the conditions being the values of strengths of the $(k-1)$th path of the nth profile and of the path with the closest delay in the $(n-1)$th profile; appropriate empirically determined correlation coefficients govern the influence these conditions exert on $a_k^{(n)}$. The mean and variance of the distribution of $a_k^{(n)}$ are also random variables, drawn from a spatial random process that reflects large-scale inhomogeneities in the multipath profile as the vehicle moves over large areas.

3) The phase $\theta_k^{(n)}$ of the kth path of the nth profile is independent of phases of other paths in the same profile, but has a distribution depending on the phase of a path with the same delay in profile $(n-1)$, if there is such a path; if no such path exists $\theta_k^{(n)}$ is uniformly distributed over $[0, 2\pi)$.

4) The spatial correlation distances of the variables just described vary considerably, ranging from less than a wavelength for the θ_k's, through tens of wavelengths for the a_k's and τ_l's, to hundreds of wavelengths for the means and variances of the a_k's.

These statistics are more fully explained in [8], [9].

D. The Simulation Program

Hashemi's simulation program SURP, based on the statistics just outlined, generates sequences of multipath profiles, as depicted in Fig. 3. If one were to examine a sequence of such profiles, he would see paths appearing and disappearing at a rate depending on the spacing of points on the vehicle's track (Fig. 3(a)). Profiles at only slightly separated geographical points would look very similar, with high correlations of path delays and strengths (and, for *very* close points, phases). Profiles at greatly separated points would not only have grossly dissimilar $\{\tau_l\}$, $\{a_k, \theta_k\}$ strings, but the gross strength statistics of these strings (e.g., the average strength of the paths in a string) would be dissimilar, reflecting the spatial inhomogeneity incorporated into the model. The "motion picture" of simulated profiles just described is in fact very much like experimental data [37].

The simulation program can be run, using empirically determined parameters, for each of the three frequencies and four areas of the original experiment. Long sequences of strings were in fact generated for each of the twelve frequency/area combinations, assuming that the points on the vehicle track are uniformly spaced by distance d. An example of such sequences is given later in Fig. 25. For various values of d, the statistics of the simulated sequences were then compared with the original empirical statistics. Excellent agreement was obtained [8], [9]. (See Fig. 4 for examples.)

It should be noted that initial simulation experiments on urban/suburban radio ranging and location systems, using a rudimentary propagation simulation program preceding SURP, gave results which compared extraordinarily accurately with actual hardware experiments [34]. In particular, it was verified that although the data upon which the simulation program is based were taken in the San Francisco Bay area, one can expect simulation results that are not correspondingly restricted geographically. For example, use of the Area-A parameters in the program led to results that are as applicable to, say, downtown New York City or Chicago as to downtown San Francisco. This initial success encouraged the development of the more elaborate simulation capability just described.

Thus the sequence generated by SURP, described above, provide a data base with which to perform accurate experiments with urban/suburban radio systems, and the results of

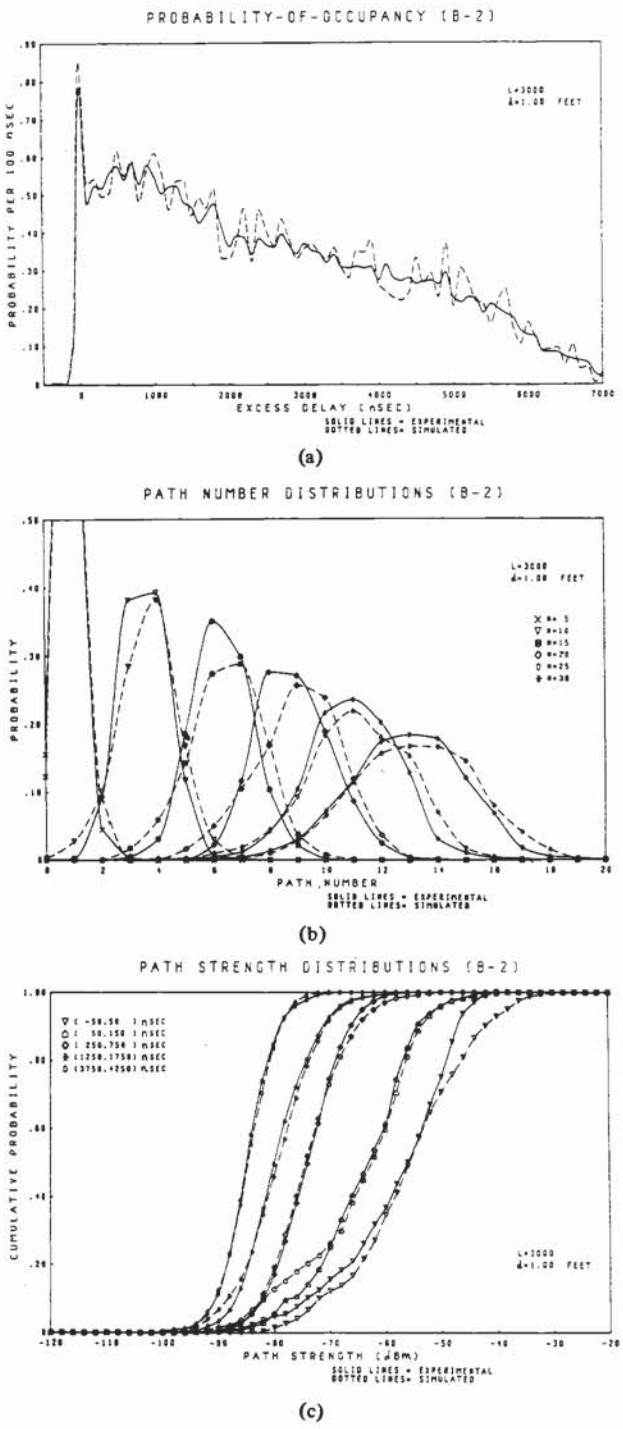

Fig. 4. Comparison of empirical statistics with statistics of simulation runs: sparse high-rise, 1280 MHz; 3000 simulation samples at 1-ft spacings. Solid curves: empirical; broken curves: simulation. (a) Ordinate is probability that a path occurs within ±50 ns of abscissa value. (b) Ordinate is probability that there are the number of paths given by the abscissa within the first N bins. (c) Ordinate is the probability that the strength of a path in the indicated delay interval is less than the abscissa value.

[3] Actually, Suzuki [25] showed that paths with small delays (beyond LOS delay) were better modeled by Nakagami distributions, but Hashemi [9] was forced to approximate these log-normally because of the complexity of the simulation program.

these experiments can be expected to have wide applicability to typical urban/suburban topographies.

III. Design of Multipath Receivers

Multipath reception is one form of diversity reception, in which information flows from transmitter to receiver via the natural diversity of multiple paths rather than via the planned diversity of multiple frequency channels, multiple antennas, multiple time slots, etc. Thus instead of regarding the multipath phenomenon as a nuisance disturbance whose effects are to be suppressed, it should be regarded as an opportunity to improve system performance.

Two bodies of work in the literature are concerned with multipath receiver design. The older (see, e.g., [1], [4], [22], [23], [27]) concentrates on the explicit diversity structure of resolvable paths; its thrust is to take advantage of this structure by optimally combining the contributions of different paths. In its simplest form, this approach ignores the intersymbol interference that can be caused when the multipath medium delays a response from a transmitted symbol into intervals occupied by subsequent symbols, an approach that is justified only when the duration of the transmitted symbol is large compared with the duration of the multipath profile.

More recently [15]–[18], equalization techniques that were developed for data transmission over telephone lines [14] have been applied to the radio multipath problem. Here, receiver design concentrates on reduction of the effects of intersymbol interference, and the diversity-combining properties of the receiver are only implicit. This approach appears most suitable when the paths are not resolvable and when the symbol duration is much smaller than the multipath profile's "spread."

A melding of the two approaches is currently being worked on by L-F. Wei of ERL, UC Berkeley. Since we are concerned here with the case in which resolvability condition (4) is satisfied, we shall in this paper pursue only the former diversity-oriented approach, as modified to take into account the deleterious effects of intersymbol interference. Instead of indulging in general and complex derivations, however, we shall present results using a tutorial "building block" approach, employing intuitive arguments that are justified by references to more formal developments in the literature.

A. The Optimal Single-Path Receiver

We start with the simple case in which the channel comprises only one path: $K = 1$ in (3). We assume initially that the path strength a_0 and delay t_0 are known ($t_0 = 0$ for simplicity), but that the carrier phase θ_0 is unknown, being a random variable, uniformly distributed over $[0, 2\pi)$.[4]

Since the absence of multipath implies the absence of intersymbol interference (a point we discuss more fully later), we can concentrate on the reception of a single symbol, say over the interval $0 \leqslant t < T$. Knowledge of this interval of course implies some sort of synchronization procedure at the receiver, a question discussed below.

Suppose the received signal $r(t)$ is as in (2), with $0 \leqslant t < T$, and where, in (3), $K = 1$, $t_0 = 0$, a_0 is known, and θ_0 is random as described above. The transmitted signal $s(t)$ of (1) can be any of M possible waveforms

$$s_i(t) = \mathrm{Re}\,[\sigma_i(t) \exp(j\omega_0 t)], \quad i = 1, \cdots, M. \tag{5}$$

We assume that the transmitter has chosen among the s_i at random with equal probability and that the s_i have equal energy:

$$\int_0^T s_i^2(\tau)\, d\tau = \mathcal{E}, \quad \text{for all } i. \tag{6}$$

The additive noise $n(t)$ of (2) is for simplicity assumed to be white and Gaussian, although non-Gaussian noise is also common in urban radio communication. (See [39] for a comprehensive survey of urban noise.)

It is well known that the optimal receiver—i.e., the receiver that decides which s_i was sent with minimum probability of error—has the form depicted in Fig. 5 (see, e.g., [36]). As shown there, $r(t)$ is passed through a bank of M filters, "matched" respectively to $s_i(t)$, $i = 1, \cdots, M$, i.e., having impulse responses $s_i(T - t)$, $0 \leqslant t < T$ [29]. The filter outputs are envelope detected and the envelopes sampled at $t = T$ and compared. The index $i = 1, \cdots, M$ of the largest sample is the receiver's output.

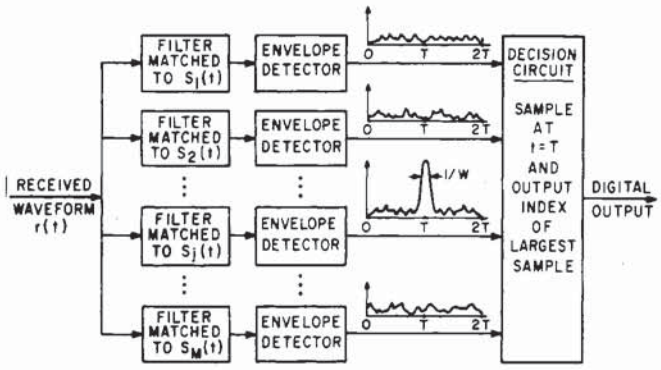

Fig. 5. Optimal noncoherent-phase receiver for single-path channel. (Equiprobable, equienergy signals, Gaussian noise.)

In Fig. 5, we have shown the outputs of the envelope detectors when $s_j(t)$ is the transmitted signal and when the received noise component $n(t)$ is negligible, assuming that the s_i have been "well chosen." This latter assumption means that if we define complex correlation function

$$\gamma_{ik}(t) \triangleq \int_0^T \sigma_i^*(\tau)\, \sigma_k(\tau - t)\, d\tau, \qquad i, k = 1, \cdots, M, \quad |t| \leqslant T \tag{7}$$

then [27]

$$|\gamma_{ik}(t)| \ll 2\mathcal{E}, \quad \text{all } k \neq i, \quad \text{all } i \tag{8a}$$

$$|\gamma_{ii}(t)| \ll 2\mathcal{E}, \quad \text{for } |t| > \frac{1}{W}, \quad \text{all } i \tag{8b}$$

where W is the bandwidth shared by all s_i, and, optimally but not necessarily,

$$\gamma_{ik}(0) = 0, \quad \text{all } k \neq i, \quad \text{all } i. \tag{8c}$$

In sketching the envelope detector outputs, we have also assumed that $TW \gg 1$, i.e., the signals are of the so-called

[4] Random path phases are assumed throughout this paper, since these generally change too rapidly in the mobile environment to make use of coherent-receiver techniques.

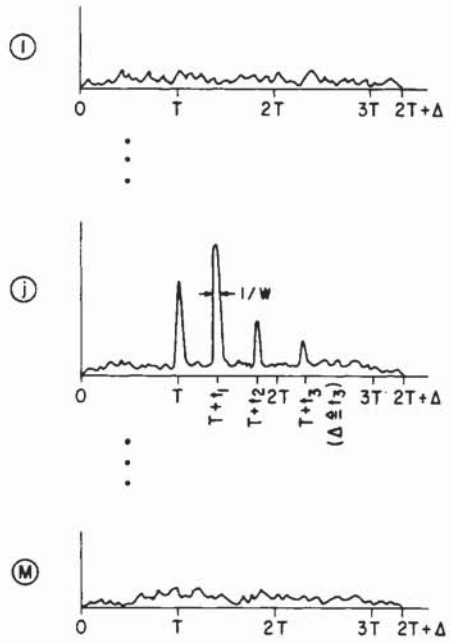

Fig. 6. Envelope detector output waveforms (small-noise case) for the receiver of Fig. 5; four-path channel.

spread-spectrum type [6]. None of the foregoing assumptions about the structure of the signal set $\{s_i(t)\}_{i=1}^{M}$ is necessary for the optimality of the single-path receiver of Fig. 5 to hold; but we shall invoke them when discussing multipath receivers later, as they become necessary or desirable.

The noisefree waveforms sketched in Fig. 5 are in fact given by [27]

$$e_l(t) \triangleq \tfrac{1}{2}\,|\gamma_{jl}(t-T)|, \qquad l = 1, \cdots, M, \qquad 0 \leqslant t < 2T. \tag{9}$$

Conditions (8a, b) and $TW \gg 1$ assure that the jth output envelope $e_j(t)$ consists of a sharp "mainlobe" peak surrounded by low-level "sidelobes," while all other outputs have only low-level sidelobes. By careful signal selection, (8a, b) can be satisfied with the maximum sidelobe level in all these waveforms at a factor of about $2/\sqrt{TW}$ down from the mainlobe. Typically, for $TW = 100$, this means that the maximum sidelobe is about 17 dB or more down from the mainlobe.

If condition (8c) is also satisfied, the values of $e_l(T)$ for $l \neq j$ are zero at the sampling instant $t = T$, so that—in the absence of received noise—the receiver will not make an error. If the received noise is nonzero, the probability that the lth output exceeds the jth at $t = T$ for some $l \neq j$ is also nonzero, and it is this probability (of erroneous decision) that characterizes the receiver's performance.

A final feature of Fig. 5 is important. There, we have depicted the output waveforms when a single isolated symbol is sent during $0 \leqslant t < T$. If another symbol, say $s_l(t)$, were sent immediately afterward, in $T \leqslant t < 2T$, it is clear that the response to it would occur over the interval $T \leqslant t < 3T$. The mainlobe peak in the lth output would be centered exactly at $t = 2T$, precisely when all responses from the first symbol have died out. Thus on sampling the outputs at $t = 2T$, one would be able to make a decision based on the response to the second symbol alone, whence our previous statement that no intersymbol interference occurs in this single-path case.

B. The Optimal Multipath Receiver: Known Delays

If we should attempt to use the receiver of Fig. 5 when many paths are present ($K > 1$ in (3)), we would expect from the linearity of the medium and of the matched filters that the envelope detector output waveforms will look something like those in Fig. 6. Here, we have shown a four-path situation ($K = 4$).

The lth response in Fig. 6 is the envelope of the superposition of the several paths' contributions, and, when noise is absent, can be shown from (3) and (7) to be of the form [27]

$$e_l(t) \triangleq \frac{1}{2}\left|\sum_{k=0}^{K-1} a_k \exp(j\theta_k) \int_0^T \sigma_j^*(\tau)\, \sigma_l(\tau + T + t_k - t)\, d\tau\right|,$$
$$l = 1, \cdots, M, \qquad 0 \leqslant t < 2T + \Delta. \tag{10}$$

Under resolvability condition (4), the mainlobe peaks in the jth output $e_j(t)$ are distinct, and occur as shown at $t_0 = 0$, t_1, t_2, and $t_3 = \Delta$.[5] The heights of these peaks are proportional to the path strengths a_k. The sidelobes, both of $e_j(t)$ and of the other outputs (none of the latter having mainlobe peaks), are mixtures of sidelobes due to the several paths. We stress that Fig. 6 is drawn for the isolated transmission of a single waveform $s_j(t)$, $0 \leqslant t < T$.

The waveforms of Fig. 6 differ from those of Fig. 5 in several important respects.

1) Strong peaks are available in $e_j(t)$ at multiple times. If the decision circuit of Fig. 5 knows the values of the path delays $t_0, \cdots, t_{K-1}$, it can sample the contributions of all paths and combine them, affording the receiver the advantages of diversity reception, as discussed earlier. The ability to resolve the paths in Fig. 6 is the essence of the spread-spectrum approach. If we instead had $TW \cong 1$, the peaks in Fig. 6 would merge, and explicit diversity combination would no longer be available.

2) The sidelobe levels of all outputs is increased, since (10) shows the addition of multipath contributions.

3) The responses to the symbol sent during $0 \leqslant t < T$ now extends beyond $t = 2T$, thus overlapping with the responses to the next symbol, which is sent during $T \leqslant t < 2T$. That is, we now have intersymbol interference, caused by the multipath.

Effects 2) and 3) are deleterious, while 1) is favorable. As we shall see, however, the benefits of 1) usually far outweigh the deterioration caused by 2) and 3).

For the time being, we shall ignore the effects of intersymbol interference, and inquire into the structure of the optimum receiver for reception of a single symbol through multipath, assuming first that the path delays $\{t_k\}_0^{K-1}$ are known. However, we again assume random phases $\{\theta_k\}_0^{K-1}$, independently and uniformly distributed over $[0, 2\pi)$; we also assume that the path strengths $\{a_k\}_\theta^{K-1}$ are random, perhaps having different distributions.

Intuitively, one might expect under these conditions that the optimal receiver is still of the form of Fig. 5, but what

[5] The maximum excess delay anticipated in the channel—i.e., $\max_{t_{K-1}} \cdot \min_{t_0}(t_{K-1} - t_0) \triangleq \Delta$—is called the multipath spread; it is by this amount that the waveforms of Fig. 6 can spread beyond those of Fig. 5. In the four-path example of Fig. 6, it is assumed that $t_3 - t_0$ achieves this maximum.

the decision circuit now samples each of its inputs at multiple times $T + t_k$, $k = 0, \cdots, K-1$, combines these samples for each input, and compares the resulting combined values; the decision would be the index of the largest combined value. Indeed this is the case, at least when (4) and (8b) hold so that the pulses in output j of Fig. 6 are distinct [27]. However, the optimal combining law is sometimes complicated, and depends on the statistics of the path strengths.

Suppose that the sample of the lth output envelope at time $T + t_k$ is x_{lk}. (In the absence of noise $x_{lk} = e_l(t_k)$ as given by (10).) Then, if all path strengths a_k are known, the optimal[6] combining of the samples is given by [27]

$$w_l = \sum_{k=0}^{K-1} \log_e I_0 \left(\frac{2a_k x_{lk}}{N_0} \right) \tag{11}$$

where I_0 is a Bessel function and where N_0 is the channel noise power density. If, on the other hand, the kth path strength is Rayleigh distributed with mean-square strength $\psi_k \triangleq E[a_k^2]$, and all path strengths are independent,[7] the optimal combining law is [27], [30]

$$w_l = \sum_{k=0}^{K-1} \frac{\psi_k x_{lk}^2}{N_0 + \psi_k \mathcal{E}} \tag{12}$$

where $\mathcal{E}$ is the common energy of the signals s_i, given by (6). More complicated combining laws for other strength distributions are given elsewhere [3], [27], [30]. In any case, a decision is made by comparing the w_l and favoring the largest.

Note that different combining laws accentuate the various samples in different ways. In (11), for example, the samples are approximately linearly combined, since $I_0(\cdot)$ increases approximately exponentially with its argument for large argument; but samples corresponding to paths with larger strengths are given more weight. In (12), the samples are square-law combined, thus accentuating the larger samples; but all samples from paths with large mean-square strength ($\psi_k \mathcal{E} \gg N_0$) are weighted equally while samples from weaker paths are suppressed. The essence of optimal combining laws is the relative accentuation of more credible data and the relative suppression of less credible data.

C. The Optimal Multipath Receiver: Unknown Delays

As indicated in Section II, the path delays $\{t_k\}_0^{K-1}$ and the number of paths K are often random variables, not known *a priori*. In order to determine the optimal receiver for this situation, we simplify somewhat from the path-delay model described in Section II. We now assume that the t_k's are independently chosen from a single common probability density distribution $p(t_k)$, $0 \leqslant t_k \leqslant \Delta$, and their indices subsequently reordered in order of increasing t_k. This model violates the assumptions in Section II in two respects. First, the resolvability condition (4) is not always met, since it is possible that two paths will be drawn from the distribution in such a way that $|t_k - t_l| < 1/W$. However, the probability that this will occur is small if there are no intervals of length $\leqslant 1/W$ in which substantial probability is concentrated; so $p(t_k)$ must be "diffuse," without high peaks and with $W\Delta \gg 1$.[8] Second, the method of generation of τ_l strings discussed in Section II (see Fig. 2) incorporates dependences among τ_l's for neighboring l's, which implies corresponding dependences in the associated delays t_k that are not incorporated in the simplified model just broached.

These variations from reality are not substantial for purposes of deriving a receiver that will be quasi-optimal for the real channel. The density distribution $p(t_k)$ of the simplified model can be determined from the empirical data described in Section II: it is just the path-occupancy curve exemplified by Fig. 4(a), as normalized to unit area by dividing it by the average number of paths $E(K)$. Were the simplified model used to generate the τ_l strings of Fig. 2, the path-number distributions would be Poisson distributions instead of the somewhat narrower distributions exemplified in Fig. 4(b).[9]

In deriving the optimal receiver for unknown delays, we assume that path strengths a_k and a_l are independent for all $k \neq l$, a deviation from the reality that paths whose delays are not greatly different generally have correlated strengths. As with our simplified delay model, we follow our intuition in assuming that the derived receiver, based on the simplified strength model, will be close to optimal in the real world.

With these mathematical simplifications, and assuming that (8b) holds,[10] the optimal receiver structure can be easily derived [4], [27]. This receiver computes the quantities

$$w_l \triangleq \int_T^{T+\Delta} p(t - T)\, F[x_l(t), t]\, dt, \qquad l = 1, \cdots, M \tag{13}$$

where $p(\cdot)$ is the path-delay density defined above, $x_l(\cdot)$ is the output envelope of the lth filter, and $F[\cdot, \cdot]$ is a time-varying nonlinear function. The w_l's are compared and a decision made favoring the index of the largest w_l.

The nonlinearities $F[\cdot, \cdot]$ depend on the path-strength statistics. If the path strengths are known, then (cf. (11))

$$F[x_l(t), t] = I_0 \left[\frac{2a(t - T)\, x_l(t)}{N_0} \right] \tag{14}$$

where $a(t)$ is strength of a path at delay t. If the path strengths are all Rayleigh distributed, with a path at delay t having mean-square strength $\psi(t)$, then (cf. (12))

$$F[x_l(t), t] = \exp \left[\frac{\psi(t - T)\, x_l^2(t)}{N_0 + \psi(t - T)\, \mathcal{E}} \right]. \tag{15}$$

Expressions for $F[\cdot, \cdot]$ for other path-strength statistics are given in [3], [4], [27].

In general, $F[x, t]$ is positive and monotone increasing in x, and can therefore be written as

$$F[x, t] = F[0, t] + \hat{F}[x, t] \tag{16}$$

[6] Strictly, the w_l's of (11), and of (12) below, are optimal only if (4) holds and if the $\gamma_{ii}(t)$ of (7) are identically zero for $|t| > 1/W$ rather than merely satisfying (8b); for practical purposes, satisfaction of (8b) suffices.

[7] The assumption of independent path strengths is a variation from the multipath model described in the previous section, and to that extent the resulting receiver is only quasi-optimal.

[8] It is tempting to apply subsequent results to a "channel sounding" receiver, in which $p(t_k)$ becomes an *a posteriori* distribution. But such a distribution would be highly peaked, and would therefore violate this "diffuseness" condition. We shall comment further on this point later, when discussing channel-sounding receivers.

[9] See [33], Fig. 5, for comparisons of these Poisson distributions with the actual empirical distributions.

[10] Again, as for known delays, we strictly should have $\gamma_{ii}(t) \equiv 0$ for $|t| > 1/W$, all i.

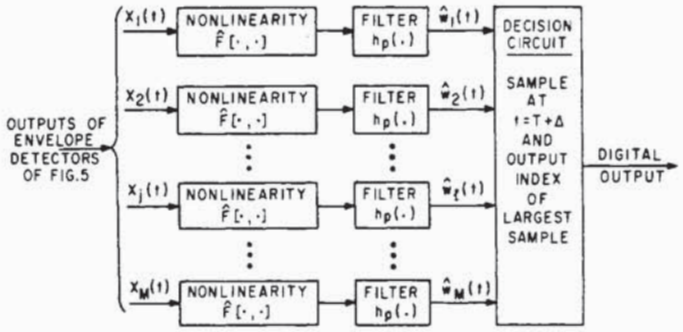

Fig. 7. Optimal noncoherent receiver for multipath channel with unknown delays. (Equiprobable, equi-energy signals; Gaussian noise; Poisson path delays, independent path strengths.)

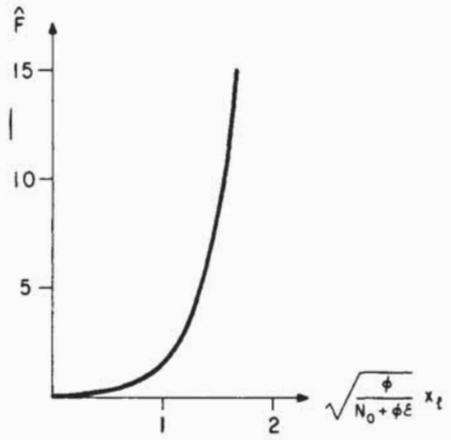

Fig. 8. The nonlinearities of Fig. 7 for Rayleigh-distributed path strengths with a common mean-square value ψ.

where $\hat{F}[x, t]$ is positive and monotone increasing in x. On substitution of (16) into (13), the $F[0, t]$ term leads to a component of w_l that is independent of l and can therefore be neglected in the comparison of the w_l's. That is, the receiver need only compare the quantities

$$\hat{w}_l \triangleq \int_T^{T+\Delta} p(t-T)\,\hat{F}[x_l(t), t]\,dt, \qquad l = 1, \cdots, M. \tag{17}$$

We note that these integrals can be realized by convolution, i.e., by generating the functions

$$\hat{w}_l(t) \triangleq \int_{t-\Delta}^{t} p[\Delta - (t-\tau)]\,\hat{F}[x_l(\tau), \tau]\,d\tau \tag{18}$$

and sampling them at $t = T + \Delta$. Thus $\hat{w}_l$ can be realized by passing $x_l(t)$ into a nonlinearity $\hat{F}$, passing the output of $\hat{F}$ into a filter with impulse response $h_p(t) = p(\Delta - t)$, and sampling the filter's output at $t = T + \Delta$. The decision circuit of Fig. 5 is therefore replaced by the circuitry of Fig. 7.

Notice that, in contradistinction to the combining laws of (11) and (12), in which the samples x_{lk}, $k = 0, \cdots, K-1$, are combined linearly or quadratically, the combining law of (18) involves extreme nonlinearities of the exponential type. For example, if the path strengths are all Rayleigh distributed with a common mean-square value ψ, then the nonlinearity

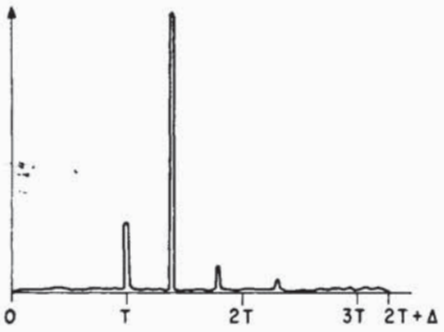

Fig. 9. Result of passage of jth waveform of Fig. 6 through the "Rayleigh" nonlinearity of Fig. 8.

in (18) is time-invariant, and of the form

$$\hat{F}[x_l, t] = \exp\left[\frac{\psi x_l^2}{N_0 + \psi \mathcal{E}}\right] - 1 \tag{19}$$

which is shown in Fig. 8. When passed through this nonlinearity, the jth envelope detector output of Fig. 6 is transformed into the waveform of Fig. 9. (On the same scale, the transformations of the other waveforms of Fig. 6 are negligibly small.)

The waveform of Fig. 9 illustrates a certain self-adaptivity implicit in (17). *A priori*, path delays are unknown. However, a large pulse in one of the $x_l(t)$'s at some instant t in $[T, T+\Delta]$ is convincing evidence that a path exists at delay $t - T$ (see Fig. 6); the larger the pulse, the more convincing is the evidence, and the more heavily the pulse is emphasized by the nonlinearity. On the other hand, whenever $x_l(t)$ is small, it is presumed to be caused by noise (or sidelobes) and it is strongly suppressed by the nonlinearity. The output of the nonlinearity thus presents data that are heavily adjusted by *a posteriori* evidence of the existence of paths. As shown by (17), these data are further weighted by the *a priori* knowledge of the probabilities of path occurrences implicit in the function $p(\cdot)$.

We stress that the illustrations in Figs. 6 and 9 are drawn for relatively large average SNR $\psi\mathcal{E}/N_0$, for which case the signal peaks are prominent and are highly emphasized with respect to the noise by the operation of $\hat{F}$. On the other hand, when $\psi\mathcal{E}/N_0$ is smaller, the noise-suppressing effect of the nonlinearities will not be great; that is, the various outputs $\hat{F}[x_l(t), t]$, $l = 1, \cdots, M$—even the jth—will be of the same scale. The signal peaks in the jth output will then contribute comparatively little to the jth integral in (17), and the receiver will be prone to error. One can see that known-path-delay receivers (such as these based on (11) and (12)), by only having to sample the envelope detector outputs at the positions of signal peaks and not the noise contributions at other instants, will perform better than unknown-path-delay receivers.

D. A DPSK Receiver

As previously mentioned, phase-coherent techniques have been avoided here because of the complexity of coherent receivers and because of the rapid time variations of path phases with vehicle motion. On the other hand, differentially coherent techniques clearly will show promise if the path phases do not vary appreciably over the interval during which two successive signals are sent; this is the usual case. Although

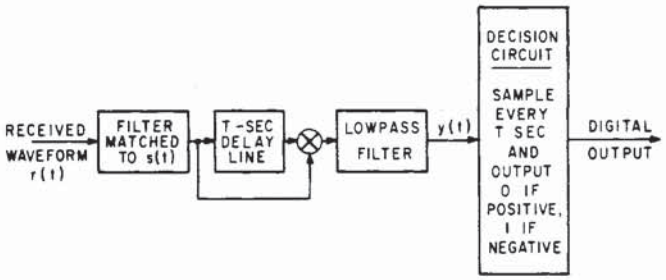

Fig. 10. Optimal DPSK receiver for the one-path case.

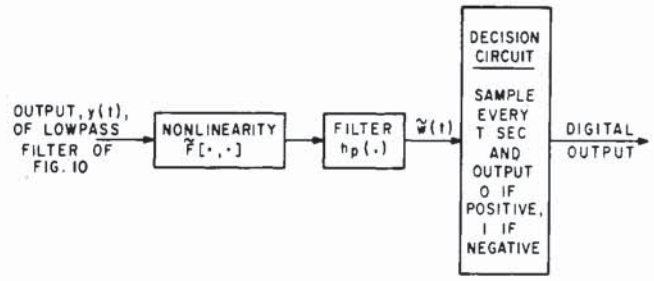

Fig. 11. Conjectured optimal DPSK receiver for multipath channel with unknown delays. (Equiprobable symbols; Gaussian noise; Poisson path delays; independent path strengths.)

the form of the optimal multipath receiver for differentially coherent signalling is not known, it is strongly suggested by that for the one-path case.

Let a signal of the form of $s(t)$ of (1) be differentially phase shift keyed: a binary 0 is sent by following a previous transmission—say $\pm s(t)$, $t \in [0, T)$—by a transmission of the same polarity in the succeeding interval—$\pm s(t-T)$, $t \in [T, 2T)$; a binary 1 is sent by changing polarity—$\pm s(t)$ followed by $\mp s(t-T)$. In the single-path case, the received waveform in $[0, T)$ is (cf. (1)–(3), with $K = 1, t_0 = 0$)

$$r_1(t) = \pm a_0 \operatorname{Re}\left[\sigma(t) \exp(j\omega_0 t) \exp(j\theta_0)\right] + n_1(t), \qquad 0 \leqslant t < T \quad (20)$$

where $n_1(t)$ is a noise waveform. If $d = 0$ or 1 is the data symbol sent, the received waveform in $[T, 2T)$ is

$$r_2(t) = \pm(-1)^d a_0 \operatorname{Re}\left[\sigma(t-T) \exp\left[j\omega_0(t-T)\right] \exp(j\theta_0)\right] + n_2(t), \qquad T \leqslant t < 2T \quad (21)$$

where $n_2(t)$ is a noise waveform and we have assumed that a_0 and θ_0 have not changed from their values during $[0, T)$. The optimal receiver in this case is well known [24] to have the form of Fig. 10. (The low-pass filter in Fig. 10 serves only to eliminate the double-frequency terms generated by the multiplier.)

By performing the operations shown in Fig. 10 on the signal components of (20) and (21), i.e., neglecting the noise components, one can easily show that the output of the low-pass filter has the form

$$y(t) = \tfrac{1}{2}(-1)^d a_0^2 |\gamma(t-2T)|^2 \quad (22)$$

where

$$\gamma(t) \triangleq \int_0^T \sigma^*(\tau)\, \sigma(\tau - t)\, d\tau, \qquad |t| \leqslant T \quad (23)$$

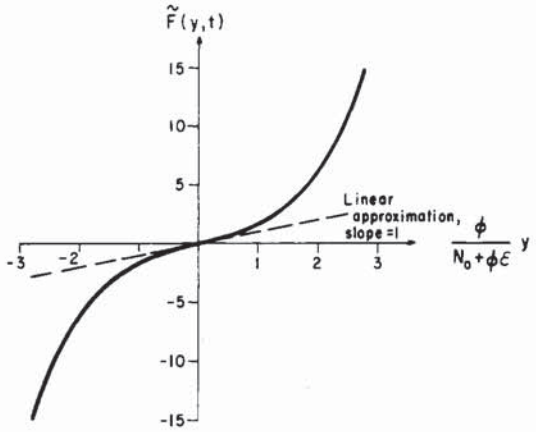

Fig. 12. The nonlinearity of Fig. 11 for Rayleigh-distributed path strengths with a common mean-square value ψ.

and $\gamma(t) \equiv 0$ elsewhere. On comparing (22), (23) with (7), (9), we see that $y(t)$ is twice the squared envelope of the response of the matched filter to the waveform $s(t)$, delayed by T seconds and keyed by $(-1)^d$. Thus in the absence of noise, the decision circuit will output exactly the input digit; when noise is present, errors will of course occur.

We now conjecture that for the case of multipath obeying the simplified model of Section III-C above, i.e., Poisson-distributed, resolvable path delays and independent path strengths, the optimal DPSK receiver bears the same relationship to Fig. 10 as the receiver of Fig. 7 bears to that of Fig. 5. More precisely, we conjecture that the optimal receiver has the form of Fig. 11. There, the nonlinearity

$$\tilde{F}(y, t) \triangleq \hat{F}(\sqrt{|y|}, t) \operatorname{sgn} y \quad (24)$$

is a bipolar version of $\hat{F}$, adjusted for the fact that the nonlinearity's input is related to the *square* of the matched filter output envelope, rather than, as in Fig. 7, the envelope itself. A graph of $\tilde{F}$ for the $\hat{F}$ of (19) is shown in Fig. 12; compare this to Fig. 8.

The samples taken every T sec by the decision circuit in Fig. 11 are timed to capture the extrema of the output of the path integrating filter $h_p(\cdot)$. Fig. 13 shows some appropriate waveforms illustrating this point. In the absence of noise, the output $y(t)$ of the product detector of Fig. 10, and therefore the input to the nonlinearity in Fig. 11, is approximately[11] of the form (cf. (22))

$$y(t) = \frac{1}{2}(-1)^d \sum_{k=0}^{K-1} a_k^2 |\gamma(t - 2T - t_k)|^2, \qquad 2T \leqslant t \leqslant 2T + \Delta \quad (25)$$

where Δ is, as before, the multipath spread. A sequence of such noiseless $y(t)$'s is shown in Fig. 13(c), for the input symbol sequence $10110\cdots$. The corresponding outputs of $\tilde{F}$ and $h_p(\cdot)$ are shown in Fig. 13(d) and (e), assuming

[11] In (25), we have assumed that the sidelobes of $\gamma(t)$ of (23) satisfy a condition of the form of (8a), so that "interpath interference" is negligible; i.e., the sidelobes due to path l are small at the peak due to path k, $l \neq k$, $l = 0, \cdots, K-1$. We have also neglected intersymbol interference, i.e., assumed that the sidelobes due to all paths in one signaling interval are negligible insofar as they extend into adjacent intervals. We return to the questions of interpath and intersymbol interference below.

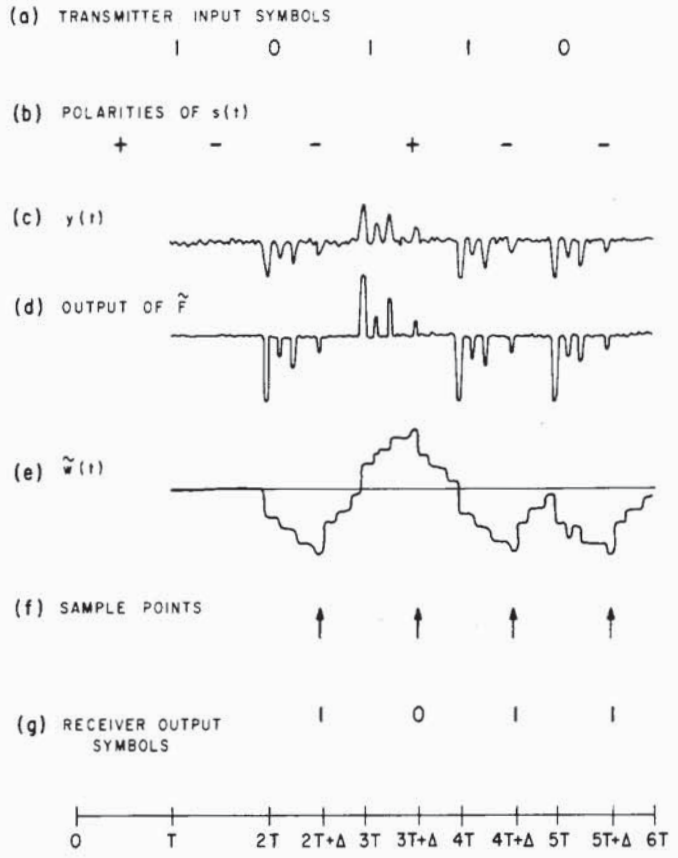

Fig. 13. Symbols and waveforms illustrating the operation of the DPSK multipath receiver of Fig. 11.

that

$$h_p(t) = \begin{cases} 1, & 0 \leqslant t \leqslant \Delta \\ 0, & \text{elsewhere.} \end{cases} \tag{26}$$

The output of $h_p(\cdot)$ is sampled at instants $nT + \Delta$, $n = 2, 3, \cdots$, and leads to the receiver outputs shown; these are delayed by $T + \Delta$ seconds from the corresponding input symbols. Of course, when noise is present, some of the output symbols will differ from the associated input symbols.

E. Channel-Sounding Receivers

Up until this point, our discussion of receiver design has been based upon *a priori* statistical knowledge of the channel. In many situations, measurements can be made of channel characteristics by use of sounding signals that enable the derivation of *a posteriori* statistics. Such sounding signals might be special signals used for sounding only, or might be the data signals themselves; in the latter case, sounding and data transmission occur simultaneously.

One's first impulse is simply to use the receiver structures discussed above for the case of unknown delays, but to base the characteristics of $\hat{F}$, $\tilde{F}$, and $h_p(\cdot)$ in Figs. 7 and 11 on *a posteriori* rather than *a priori* statistics. This would in fact be appropriate with regard to the path-strength distributions and the nonlinearities $\hat{F}$ and $\tilde{F}$ they determine. However, as indicated in footnote 8, as soon as the sounding signals enable very accurate estimation of the path delays, the diffuseness condition on the path-arrival distribution $p(t_k)$ no longer holds, and the derivation leading to (17) breaks down. Although expressions for optimal receivers using nondiffuse *a posteriori* delay distributions can be derived, they and the resulting receivers become inordinately and unnecessarily complicated.

An alternative approach is usually used. In this approach, it is assumed that sounding results in extremely accurate estimates of the path variables $\{t_k\}$, $\{a_k\}$, $\{\theta_k\}$, or at least of the delays and strengths, if not the phases. These estimates are then assumed to be exact, and used as parameters in a receiver that assumes exact knowledge of the associated variables.

In many cases, estimates of $\{\theta_k\}$ are not deemed worth making, either because of the complexity of the resulting receiver or—especially in the mobile receiver context—because these phase shifts change too rapidly to be tracked and used effectively. Therefore, we discuss here only noncoherent channel-sounding receivers that make use only of path-strength and path-delay estimates.

The "optimal" M'ary strength/delay-estimating receiver that follows the philosophy just described is clearly based on (11). The quantities

$$w_l = \sum_{k=0}^{K-1} \log_e I_0\left(\frac{2\hat{a}_k \hat{x}_{lk}}{N_0}\right) \tag{27}$$

must be calculated, where $\hat{a}_k$ is the estimate of the strength of the kth path and $\hat{x}_{lk}$ is a sample of the lth matched filter output envelope at $t = T + \hat{t}_k$, $\hat{t}_k$ being the estimate of the kth path's delay. The index $(l = 1, \cdots, M)$ for which w_l is maximum is the receiver's digital output. If the paths are strong enough with respect to the noise to be measured accurately, which is our assumption, then (27) can be approximated by

$$w_l \cong \frac{2}{N_0} \sum_{k=0}^{K-1} \hat{a}_k \hat{x}_{lk} \tag{28}$$

since $\log_e I_0(x) \cong x$ for large x. This approximation is the optimal linear diversity combiner of Brennan [2], and we shall use it henceforth.

The linear combiner of (28) can be realized through use of a transversal filter, as shown in Fig. 14. This filter incorporates a delay line Δ seconds long, which is tapped at least every $1/W$ seconds, for a minimum of $W\Delta$ taps. The input to the transversal filter is the output envelope of a matched filter, say $x_j(t)$ of Fig. 6. The output of the transversal filter is a weighted sum of certain tap outputs, the taps that are included in the sum depending on the path delay estimates $\hat{t}_k$.

The estimates $\hat{t}_k (k = 0, \cdots, K - 1)$ are used to turn on the amplifiers of those taps having the delays (measured from the *right-hand* end of the line) that most closely approximate the $\hat{t}_k$'s; i.e., K of the tap amplifiers are activated. The gains of the activated tap amplifiers are then set to be proportional to the associated strength estimates $\hat{a}_k$. Amplifier gains are shown in Fig. 14 for the four-path response assumed.

To explain how the transversal filter works, we have shown in Fig. 14 the voltage profile along the delay line that would occur if the delay line's input were the jth matched filter output envelope $x_j(t)$ of Fig. 6; this profile moves to the right with time and is shown at the instant $t = T + \Delta$. At this instant, signal peaks in the profile lie at delays t_0, t_1, $\cdots$, t_{K-1}, as measured from the line's right-hand end; these are shown in Fig. 14 for $t_0 = 0$ and $K = 4$, assuming that $t_3 = \Delta$, Δ being the maximum excess delay (beyond t_0) anticipated in the channel. If the delay estimates $\hat{t}_k$ are accurate, the activated taps will sample the profile close to these peaks, so at time $t = T + \Delta$ the transversal filter's out-

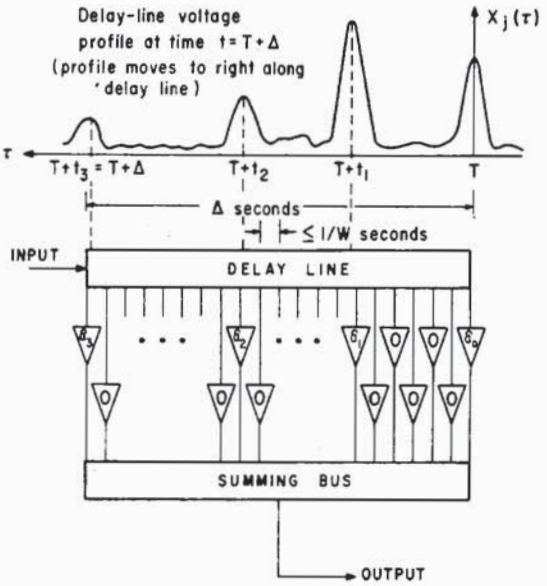

Fig. 14. A transversal filter used in realizing (28).

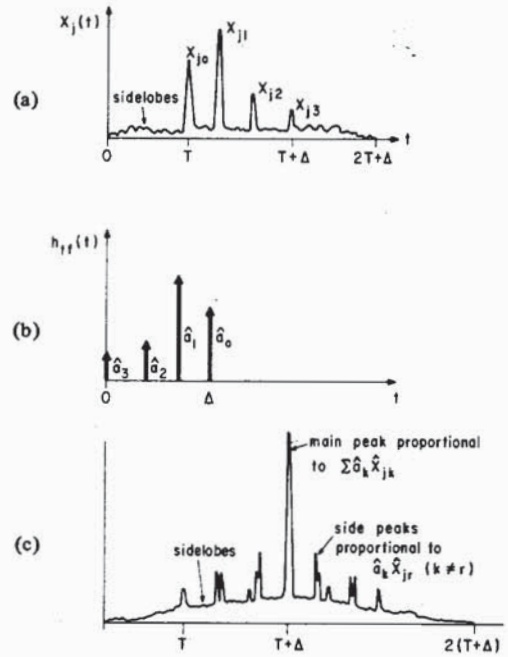

Fig. 15. Illustration of the operation of the transversal filter of Fig. 14: (a) Filter input; (b) Filter impulse response; (c) Filter output, obtained by convolving (a) and (b).

put will be approximately

$$\sum_{k=0}^{K-1} \hat{a}_k \hat{x}_j(T + \hat{t}_k) \cong \sum_{k=0}^{K-1} \hat{a}_k \hat{x}_{jk} \tag{29}$$

which is proportional to w_l, $l = j$, of (28).

Actually, the transversal filter is itself a matched filter of sorts. Note that the low-pass equivalent of the channel's impulse response, i.e., that relating $\sigma(t)$ and $\rho(t)$ of (1) and (3), is

$$h_m(t) = \sum_{k=0}^{K-1} a_k \exp(j\theta_k)\, \delta(t - t_k). \tag{30}$$

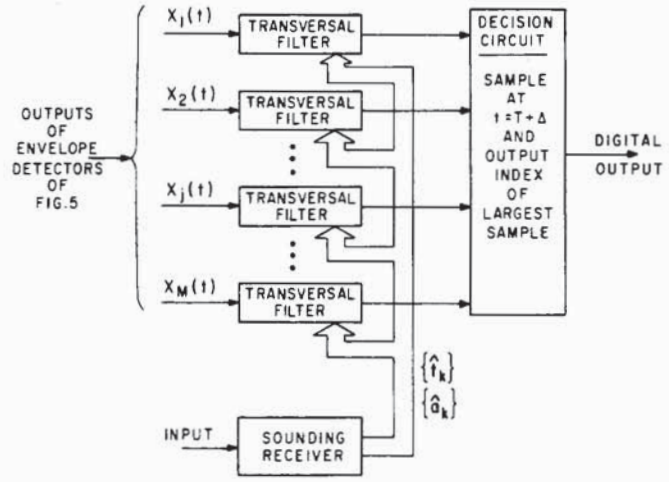

Fig. 16. A channel-sounding M'ary receiver (RAKE).

On the other hand, the impulse response of the transversal filter can clearly be written as

$$h_{tf}(t) = \sum_{k=0}^{K-1} \hat{a}_k \delta(t - \Delta + \hat{t}_k)$$

$$= \sum_{k=0}^{K-1} \hat{a}_k \delta(\Delta - t - \hat{t}_k). \tag{31}$$

The transversal filter is therefore matched to an estimate of the magnitude of the low-pass-equivalent channel impulse response.[12]

As $x_j(t)$ moves to the right in Fig. 14, the transversal filter convolves $x_j(t)$ with $h_{tf}(t)$, shown in Figs. 15(a) and 15(b), respectively, producing an output like that shown in Fig. 15(c). The main peak of this output occurs when $t = T + \Delta$, i.e., when $x_j(t)$ is aligned as in Fig. 14, with its peaks all located at activated taps. This main peak is proportional in height to (29). The output also has minor side peaks proportional to $\hat{a}_k \hat{x}_{jr} (k = 0, 1, 2, 3; r \neq k)$ and sidelobes accumulated from convolution of $h_{tf}(t)$ with the sidelobes of $x_j(t)$. It is clear that we need to sample only the main peak, to obtain (29).

A complete M'ary channel-estimating receiver can therefore be depicted as in Fig. 16. Each envelope detector output $x_l(t)$, $l = 1, \cdots, M$, enters a transversal filter of the form of Fig. 14, the parameters of which are driven by the estimates $\{\hat{t}_k\}$, $\{\hat{a}_k\}$ available from a sounding receiver. At time $t = T + \Delta$, the transversal filters' outputs are sampled and compared, and a decision made favoring the index of the largest. Such a receiver has been called a RAKE receiver [23] because of the tooth-like structure of the taps on the transversal filter's delay line.

The sounding receiver of Fig. 16 can itself be structured as a cascade of a matched filter, envelope detector and tapped delay line, where the matched filter is matched to a known waveform, perhaps containing more energy and lasting longer

[12] As discussed later in Section IV (see Fig. 20), if phase-coherent techniques were used, the transversal filter would become a bandpass filter matched to an estimate of the channel impulse response itself, i.e., the summand in (31) would contain the factor $\exp(-j\hat{\theta}_k)$. The cascade of the receiver's signal matched filter and the transversal matched filter would then form a receiver whose filter is matched to an estimate of the actual *received* signal, as modified by the channel.

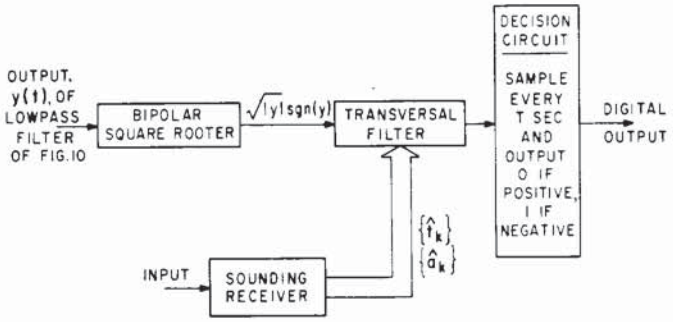

Fig. 17. A channel-sounding DPSK receiver.

than the data signals s_j. Prior to data transmission (and during it, if the channel changes rapidly enough), the sounding receiver "listens" for its signal. When the signal is received, the matched-filter output envelope will have multiple peaks, like the jth waveform of Fig. 6. This waveform will progress down a tapped delay line like that in Fig. 14. A threshold is triggered when the first peak reaches the line's right end, at which moment the voltages at each tap are sampled and held if they exceed another threshold, or set to zero if they do not. The frozen tap voltages, which are proportional to the path strengths at the tap's delays, are then used to set the gains of the associated taps in the data receiver's transversal filters.

A self-adaptive version of this receiver uses the data signals themselves for sounding. At the time of a decision favoring, say, signal j, the tap voltages of the jth transversal filter are frozen, just as in the sounding receiver discussed above; these voltages are then used to set the corresponding tap gains of all the transversal filters.[13] This self-adaptive version can be started by using a threshold triggering device of the type used in the separate sounding receiver.

We note that the sounding mechanism also performs a receiver synchronizing function, which, as previously mentioned, we have thus far ignored. Triggering of the threshold on the rightmost tap, in either the separate-sounding or self-adaptive realization, starts a clock that subsequently supplies properly timed sampling pulses to the decision circuit.

Finally, we note that a RAKE-like DPSK receiver can be structured along the same principles. This is shown in Fig. 17. Since the input in Fig. 17 is akin to the square of the inputs of Fig. 16, we have inserted a bipolar square-root operation before the transversal filter in the DPSK realization.

F. Intersymbol Interference

Heretofore, our discussion has ignored the effects of intersymbol interference by concentrating on isolated single transmissions (see, e.g., Fig. 6). Even in the DPSK case, where information is sent via the agreement or disagreement of the polarities of two successive transmissions, these transmissions were assumed to be sufficiently long or sufficiently spaced so that the time dispersion caused by the multipath channel causes little or no performance degradation (see Fig. 13).

Suppose now that each transmission of a choice from the signal set requires T seconds, and that successive transmissions occur at intervals of length T_s. As indicated by (10), the outputs of the matched filters in the receivers discussed above

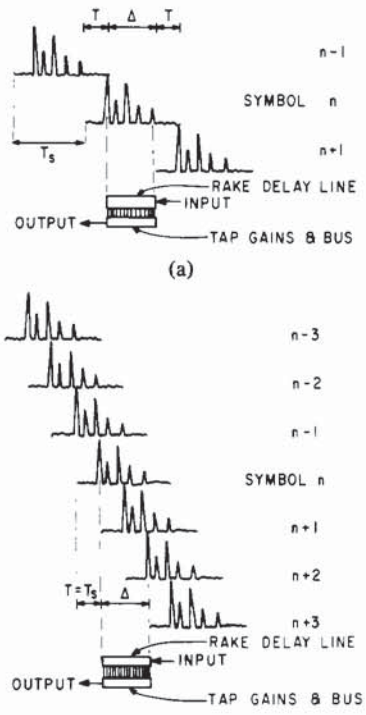

Fig. 18. Illustration of intersymbol interference (a) No intersymbol interference: $T_s \geq T + \Delta$. (b) Moderate intersymbol interference: $T_s = T$, $\Delta = 2T$.

will last $2T + \Delta$ seconds in response to each transmission of length T, raising the possibility of intersymbol interference. In order to help visualize intersymbol interference in the spread-spectrum ($TW \gg 1$) case of importance here, Fig. 18 shows sequences of output envelopes of a single matched filter in response to a periodic input of the signal to which it is matched. This diagram illustrates the interrelationships among T, T_s, and Δ.

In Fig. 18(a), we have shown a case in which there is no intersymbol interference, a situation requiring that $T_s \geq T + \Delta$. For reference, we have also shown a RAKE delay line and combiner, of length Δ; this is turned end for end compared to that of Fig. 14. The output envelopes of the response of a matched filter to three successive transmissions are shown, which should be visualized as entering the delay line from the right and moving with time to the left.[14] This output sequence is shown "frozen" at the instant at which the multipath pulses of the central (nth) transmission are perfectly aligned with the delay line and ready to be sampled. Notice that, at this instant, neither the $(n - 1)$th nor the $(n + 1)$th response is in the delay line to interfere with the nth.

In Fig. 18(b) a case of moderate intersymbol interference is shown. Here $T_s = T$ and $\Delta = 2T$, so $T_s = \frac{1}{3}(T + \Delta)$. A sequence of output envelopes in response to seven successive transmissions is shown, frozen at the instant when the multipath pulses of the central (nth) response are aligned with the delay line. However, in this case, parts of two predecessor and two successor responses ($n - 2$, $n - 1$, $n + 1$, $n + 2$) are also in the delay line, causing intersymbol interference. In general, a total of $2\lceil \Delta/T \rceil$ predecessor and successor symbols will inter-

[13] More elaborately, the nth tap gain can be set on the basis of a weighted average of the nth tap voltages held over a given number of past decisions.

[14] Of course, in practice these responses would have been superposed by the matched filter prior to envelope detection, and the actual output envelope would be a nonlinear combination of the three responses.

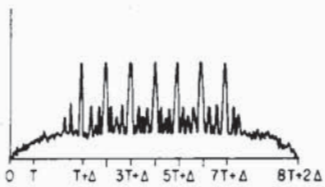

Fig. 19. The output of a RAKE transversal filter when the input consists of the seven pulse trains of Fig. 18(b).

fere with each symbol as it is sampled, where $[x]$ is the smallest integer greater than or equal to x.[15]

In order to avoid intersymbol interference completely, the condition $T_s \geq T + \Delta$ must be satisfied. Although we have some flexibility in decreasing T (subject to our requirement $TW >> 1$ and to limitations imposed on the bandwidth W), Δ is fixed by the channel. Thus, for a binary system, we cannot completely avoid intersymbol interference when the data rate is greater than roughly $1/\Delta$ b/s. For example, for binary transmission through urban multipath ($\Delta = 5$ μs, effectively), any transmission rate greater than about 200 kb/s will result in intersymbol interference, even in a spread-spectrum system.

Of course, it is well known that the effects of intersymbol interference can be ameliorated, so higher data rates can be achieved without undue deterioration of receiver performance. One approach, followed by Monsen [15]–[17], is based on classical equalization techniques developed for reduction of intersymbol interference on baseband landlines; it is particularly applicable when $TW \cong 1$ and $\Delta >> T$. In our case, when $TW >> 1$ and Δ/T is moderate, we follow a different approach, based on the RAKE receiver.

The basis of the RAKE approach is to recognize that, while multipath pulses from predecessor and successor symbols are on the RAKE delay line at the decision instant for the present symbol, as shown in Fig. 18(b), it is unlikely that they will appear at taps which are activated. Recall that the delay line has taps every $1/W$ seconds. Since $TW >> 1$, and we are now assuming that $\Delta/T > 1$, we will have $W\Delta >> 1$. There will thus be a large number, $W\Delta$, of taps. For example, if $TW = 100$ and $\Delta/T = 5$, then there are $W\Delta = 500$ taps on the delay line. On the other hand, only those taps at which pulses are expected are activated, so even if there are as many as 20 paths in the example above, only $20/500 = 2.5$ percent of the taps will be activated. These activated taps will be aligned to sample the multipath pulses of the central (nth) response in Fig. 18(b); but it is extremely unlikely that the pulses of adjacent responses on the line will also be aligned with the activated taps.

Yet another insight into the capability of the RAKE transversal filter to suppress intersymbol is given by looking at the filter's output. Although the total input to the delay line is really a nonlinear combination of the pulse trains shown in Fig. 18(b), for simplicity one can visualize the result of each pulse train sweeping to the left through the line and being convolved with the RAKE filter's impulse response, as depicted in Fig. 15. A sequence of seven such resulting convolutions, when properly combined, would look something like Fig. 19. Each of the major peaks there corresponds to the exact alignment of one of the pulse trains with the activated taps on the delay line, and it is these peaks that are sampled. The pedestal upon which the major peaks sit is composed of minor peaks, as in Fig. 15, and a general sidelobe "hash" level. We call this pedestal "multipath-induced interference."

The ability of the RAKE receiver to concentrate on the part of the matched-filter response due to the current symbol is peculiar to its tapped-delay-line structure. The integrating receivers of Figs. 7 and 11, by integrating over the interleaved responses to several symbols, cannot suppress intersymbol interference as RAKE does.

In summary, it appears that data rates much greater than $1/\Delta$ b/s can be achieved with RAKE receivers without undue deterioration of performance. We investigate this possibility both analytically and by simulation in the next several sections.

We close this subsection by noting one complication that arises in realization of a RAKE receiver when $\Delta/T > 1$. Recall that one alternative for estimating the path delays and strengths was self-adaptive, using the data signals themselves as sounding signals, and using the multipath profiles that are stretched out along the RAKE delay lines to aid in path-parameter estimation. As shown in Fig. 18(b), however, when the present (nth) signal's multipath profile is aligned with the delay line, adjacent signals can cause spurious pulses to appear on the line. These latter must be ignored in order for the RAKE receiver to avoid intersymbol interference, but—in the simple adaptive approach to path-parameter estimation outlined in the previous subsection—they also would tend to be identified as true paths and cause spurious activation of taps. Thus, when $\Delta/T > 1$, the self-adaptive approach to estimation is not straightforward. Work on self-adaptive systems with $\Delta/T > 1$, in which the data signals are used for channel estimation, is now ongoing at this Laboratory. Initial simulation results show that such systems can successfully adapt to and track a time-varying multipath profile.[16]

G. Comments on Optimality and Quasi-Optimality

From a theorist's point of view, we are in an unenviable position. Only in the case of an incoherent single-path channel disturbed solely by additive white Gaussian noise have we specified a receiver, i.e., Fig. 5, that is strictly optimal in anything approaching the real world. The multipath receivers we have discussed are not strictly optimal: either their optimality depends on invoking a large set of oversimplifying assumptions (e.g., the receivers specified by (11), (12), and (13)), or they have no sure claims to optimality at all (e.g., the receivers of Figs. 11, 16, and 17). The unfortunate fact is that we do not know the optimal receiver structure for the real-world multipath channels described in Section II, nor for nonideal signal sets, and such structures are unlikely to be analytically derivable. We are thus deprived of the theorist's benchmark: the knowledge of the optimal performance, beyond which no receiver can reach.

Nonetheless, we rely on a pragmatic faith that the multipath receivers we have specified, by virtue of the intuitive reasonableness of their derivation, cannot be too far off the mark, whence the appellation "quasi-optimal." That is, we believe their performance to be within a very few decibels of the unknown benchmark of optimality. We shall in a later section present evidence that supports this belief.

[15] In the DPSK case shown in Fig. 13, $T_s = T$ and $\Delta/T < 1$, so there is intersymbol interference by only one successor and one predecessor. The interference is due only to the sidelobes of the multipath pulses in neighboring transmission intervals, rather than to the pulses themselves as in Fig. 18(b), and the interference can be deemed negligible.

[16] Private communications from L-F. Wei.

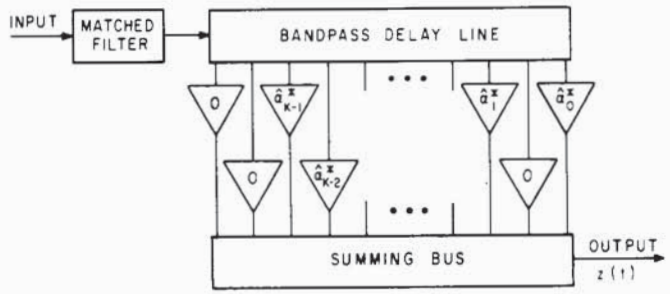

Fig. 20. Bandpass RAKE system used for "equivalent noise" analysis.

IV. Simplified Analysis of Multipath-Induced Interference

We have just concluded by a number of heuristic arguments that, even if $T_s \ll T + \Delta$, a RAKE receiver will work satisfactorily, despite multipath-induced interpath and intersymbol interference.[17] In the present section, we present an analysis that bolsters our confidence in this conclusion.

A. A Simplified Model

For simplicity, we consider a coherent receiver, since the noncoherent receivers discussed in Section III lead to complicated nonlinear analysis. More specifically, we analyze a binary, coherent PSK system whose receiver filters are shown in Fig. 20. Here, a bandpass matched filter is followed by a bandpass transversal filter, rather than (as previously) by a cascade of an envelope or DPSK detector and a low-pass transversal filter. As in the case of the low-pass transversal filter of Fig. 14, the tap gains in Fig. 20 are set by estimates of path strengths.[18] Now, however, these gains not only weight the tap outputs by estimates $\hat{a}_k$ of the path strengths, but also try to correct for the paths' phase shifts θ_k by phase shifting the tap outputs in the opposite directions, by amounts $-\hat{\theta}_k$. (See footnote 12.) We have written the nonzero gains in Fig. 20 in complex form

$$\hat{\alpha}_k^* = \hat{a}_k \exp(-j\hat{\theta}_k). \tag{32}$$

The lowpass-equivalent impulse response of the transversal filter is clearly of the form (cf. (31))

$$\hat{h}_{tf}(t) = \sum_{k=0}^{K-1} \hat{\alpha}_k^* \delta(\Delta - t - t_k). \tag{33}$$

We therefore see that $\hat{h}_{tf}(t)$ would be matched to the channel's impulse response, given by (30), if the estimates were perfect, i.e., if $\hat{a}_k = a_k$, $\hat{\theta}_k = \theta_k$, and $\hat{\tau}_k = t_k$, all k.

We continue in low-pass-equivalent form in the frequency domain. Let $\sigma(t)$, $0 \leq t \leq T$, be the low-pass equivalent of a signal transmitted through the channel (cf. (1)) and let the Fourier transform of $\sigma(t)$ be $S(f)$. Disregarding channel noise for the moment, the channel output then has spectrum $S(f)H_m(f)$, where $H_m(f)$ is the Fourier transform of $h_m(t)$ of (30), i.e.,

$$H_m(f) = \sum_{k=0}^{K-1} \alpha_k \exp(-j2\pi f t_k) \tag{34}$$

where $\alpha_k = a_k \exp(j\theta_k)$. The matched filter in Fig. 20 has low-pass-equivalent impulse response $\sigma(T - t)$ and transfer function $S^*(f) \exp(-j2\pi fT)$, so its output has spectrum $|S(f)|^2 H_m(f) \exp(-j2\pi fT)$. The transversal filter has transfer function

$$\hat{H}_{tf}(f) = \sum_{k=0}^{K-1} \hat{\alpha}_k^* \exp[-2\pi f(\Delta - \hat{\tau}_k)] \tag{35}$$

(the Fourier transform of (33)), whence its output has spectrum

$$\begin{aligned} W(f) &= |S(f)|^2 H_m(f) \hat{H}_{tf}(f) \\ &= |S(f)|^2 \sum_{k=0}^{K-1} \sum_{l=0}^{K-1} \alpha_k \alpha_l^* \\ &\quad \cdot \exp[-j2\pi f(t_k - \hat{\tau}_l)] \\ &\quad \cdot \exp[-j2\pi f(T + \Delta)]. \end{aligned} \tag{36}$$

We assume for simplicity that the channel-sounding procedure has led to very good estimates, so we set $\hat{a}_k = a_k$, $\hat{\theta}_k = \theta_k$ (hence, $\hat{\alpha}_k = \alpha_k$), and $\hat{\tau}_k = t_k$.[19] We also shift the time origin to the right by $T + \Delta$ seconds to eliminate the factor $\exp[-j2\pi f(T + \Delta)]$ in (36). Then (36) becomes

$$W(f) = |S(f)|^2 \sum_{k=0}^{K-1} \sum_{l=0}^{K-1} \alpha_k \alpha_l^* \exp[j2\pi f(t_k - t_l)]. \tag{37}$$

The corresponding time waveform is the inverse Fourier transform of $W(f)$, i.e.,

$$w(t) = \sum_{k=0}^{K-1} \sum_{l=0}^{K-1} \alpha_k \alpha_l^* \gamma(t - t_k + t_l), \qquad |t| \leq T + \Delta \tag{38}$$

where $\gamma(t)$ is the inverse Fourier transform of $|S(f)|^2$, and is given by (23).

For the case in which $\sigma(t)$ is sent only once through the channel, (38) is the low-pass-equivalent output of the transversal filter, shifted so that its peak lies at $t = 0$. (The true bandpass output is $\frac{1}{2} Re[w(t) \exp(j\omega_0 t)]$ and the output envelope, $\frac{1}{2}|w(t)|$, has a shape like that depicted in Fig. 15(c), where the central peak is now centered at $t = 0$.) If we now suppose that an infinitely long PSK sequence, $\sum_{n=-\infty}^{\infty} d_n \sigma(t - nT)$, $d_n = \pm 1$, is sent through the channel, the corresponding low-pass-equivalent output of the transversal filter will be

$$v(t) = \sum_{n=-\infty}^{\infty} d_n w(t - nT). \tag{39}$$

The output envelope, $\frac{1}{2}|v(t)|$, will now look like Fig. 19, where the result of only seven transmissions is shown. The central peak in Fig. 19 would correspond to the $n = 0$ term in (39), now centered on $t = 0$.

The analysis in this section is concerned with the degradation in performance caused by the multipath-induced interference. Ideally, this degradation should be measured in terms of error probability. However, the multipath statistics that govern the error probability are so complicated as to make this ideal goal unattainable. Instead, we shall perform an "equivalent noise" analysis.

[17] See footnote 11, for a definition of these terms.

[18] Unlike the case in Fig. 14, in Fig. 20 the largest estimated excess delay $\hat{t}_{K-1} - \hat{t}_0$ is less than Δ.

[19] As seems obvious, and is shown in Appendix C, if the channel-sounding signal's energy is much greater than the data signals' energy, this is a reasonable assumption.

We concentrate on the central peak in $v(t)$, i.e., on

$$v(0) = \sum_{n=-\infty}^{\infty} d_n\, w(-nT). \tag{41}$$

Noting from (38) that $w(t)$ is nonzero only in $|t| \leqslant T + \Delta$, we see that (41) only has $2N+1$ nonzero terms, where $N = \lceil \Delta/T \rceil$ is the smallest integer greater than or equal to T/Δ. Thus using (38), (41) becomes

$$v(0) = \sum_{n=-N}^{N} d_n \sum_{k=0}^{K-1} \sum_{l=0}^{K-1} \alpha_k \alpha_l^* \gamma(nT - t_k + t_l). \tag{42}$$

This is the signal component of the transversal filter output at $t = 0$. A component due to channel-noise, call it $n(0)$ adds to this, leading to a total output

$$z(0) = v(0) + n(0). \tag{43}$$

Our approach to evaluating the effect of multipath-induced interference is to determine how much its presence increases the variance of $z(0)$ above the value contributed by $n(0)$, i.e., how much "equivalent channel noise" is added by intersymbol interference.

In order to proceed, we make a number of simplifying assumptions about the multipath statistics that are akin to those made in Section III in deriving "optimal" receiver structures:

1) $\{a_k\}_0^{K-1}$, $\{\theta_k\}_0^{K-1}$ and $\{t_k\}_0^{K-1}$ are independent sets of random variables and all variables in each set are independent of each other;
2) the number of paths K is independent of $\{a_k\}_0^{K-1}$, $\{\theta_k\}_0^{K-1}$ and $\{t_k\}_0^{K-1}$;
3) all t_k's are equidistributed over $[0, \Delta]$ with probability density $p(t_k)$; see the discussion in Section III-C;
4) each θ_k is uniformly distributed over $(0, 2\pi]$.

As previously noted, these assumptions depart somewhat from reality, but will serve for the present heuristic analysis.

We also assume that the data sequence $\{d_n\}_{-N}^{N}$ consists of independent binary values, being +1 or −1 with equal probability, and that the channel noise is independent of the multipath variables.

B. The variance of z (0)

Attacking the signal component $v(0)$ in (43) first, suppose that the desired datum in $v(0)$, i.e., d_0, is +1. Then, using the assumptions discussed above, it is straightforward to show that

$$E[v(0)]\,\big|_{d_0=+1} = \gamma(0) E_K\left[\sum_{k=0}^{K-1} \overline{|\alpha_k|^2}\right] = 2\mathcal{E}A^2. \tag{44}$$

Here, an overbar denotes "expectation," and E_K denotes expectation over the random variable K. We have used the fact that $\gamma(0) = 2\mathcal{E}$, $\mathcal{E}$ being the energy in the transmitted signal $s(t) = Re[\sigma(t) \exp(j\omega t)]$; we have also let

$$A^2 \triangleq E_K\left[\sum_{k=0}^{K-1} \overline{|\alpha_k|^2}\right]. \tag{45}$$

Not so straightforwardly, one can show (see Appendix A) that, when $W\Delta \gg 1$,

$$\text{var}\,[v(0)]\,\big|_{d_0=+1} = (2\mathcal{E})^2 B^2 + \left[\int_{-\infty}^{\infty} |S(\nu)|^4 d\nu\right]\left[\sum_{n=-N}^{N} q(nT)\right] C^2 \tag{46}$$

where

$$B^2 = E_K\left[\sum_{k=0}^{K-1} \overline{|\alpha_k|^4} - \sum_{k=0}^{K-1} \overline{|\alpha_k|^2}^2\right] = E_K\left[\sum_{k=0}^{K-1} \text{var}\,(|\alpha_k|^2)\right] \tag{47}$$

$$C^2 = E_K\left[\sum_{k=0}^{K-1} \sum_{\substack{l=0 \\ k \neq l}}^{K-1} \overline{|\alpha_k|^2}\;\overline{|\alpha_l|^2}\right] = E_K\left[\left(\sum_{k=0}^{K-1} \overline{|\alpha_k|^2}\right)^2 - \sum_{k=0}^{K-1} \overline{|\alpha_k|^2}^2\right] \tag{48}$$

and

$$q(t) = \int_0^{\Delta} p(\tau)\, p(\tau - t)\, d\tau. \tag{49}$$

The variance in (46) is, in fact, independent of the condition $d_0 = +1$. It is important to note that the two contributions to this variance have distinctly different interpretations. The first term is independent of N and would be present even if there were no multipath-induced interference; it reflects the variation of $v(0)$ around its mean due to the fluctuations in the strengths of the paths that have been combined by the RAKE receiver to decide on the datum d_0 in $v(0)$. The second term is due to multiple-induced interference; it reflects the fluctuations in $v(0)$ due to the presence of both interpath interference on the "present" transmission ($n = 0$) and intersymbol interference from neighboring transmissions ($n \neq 0$). The second term will vanish only if, with probability one, there is but one path ($K = 1$) in (48).

We next consider the term $n(0)$ in (43). It has zero mean, so its mean adds nothing to (44). Its variance is derived in Appendix B. Since $v(0)$ and $n(0)$ are assumed to be independent, the variance of $z(0)$ becomes

$$\text{var}\,[z(0)] = \text{var}\,[v(0)] + \text{var}\,[n(0)] = (2\mathcal{E})^2 B^2 + \left[\int_{-\infty}^{\infty} |S(\nu)|^4 d\nu\right]\left[\sum_{n=-N}^{N} q(nT)\right] C^2 + 4\mathcal{E}N_0 A^2 \tag{50}$$

where N_0 is the (single-ended) power density of the channel noise, assumed to be white.

C. A Measure of Performance Degradation

As mentioned, only the second term in (50) is due to the multipath-induced interference of interest to us here. In the next section, for the purpose of estimating error probabilities, we shall model this interference as approximately Gaussian,

equivalent to an additional amount of channel noise. In this framework, multipath-induced interference degrades system performance by the same amount as would an increase in channel noise power by a factor of

$$D = 1 + \frac{C^2}{4\mathcal{E}N_0A^2}\left[\int_{-\infty}^{\infty}|S(\nu)|^4 d\nu\right]\left[\sum_{n=-N}^{N} q(nT)\right]. \quad (51)$$

We now specialize (51) by some additional assumptions. First, suppose that $|S(f)|^2$ is flat over the band $|f| \leqslant W/2$ and zero elsewhere. Then, since the integral of $|S(f)|^2$ is equal to $2\mathcal{E}$,

$$|S(f)|^2 = \frac{2\mathcal{E}}{W}, \quad |f| \leqslant \frac{W}{2} \quad (52)$$

and

$$\int_{-\infty}^{\infty}|S(f)|^4 df = \frac{4\mathcal{E}^2}{W}. \quad (53)$$

Second, suppose that $\Delta >> T$, so that we can use the following approximation:

$$\sum_{n=-N}^{N} q(nT) \cong \frac{1}{T}\int_{-\Delta}^{\Delta} q(t)dt$$

$$= \frac{1}{T}\left[\int_0^{\Delta} p(\tau)\,d\tau\right]^2 = \frac{1}{T}. \quad (54)$$

Finally, assume that all paths have identical strength statistics, so $\overline{|\alpha_k|^2} = \overline{|\alpha|^2}$, all k, whence

$$A^2 = \overline{K}\ \overline{|\alpha|^2} \quad (55)$$

$$C^2 = (\overline{K^2} - \overline{K})\ \overline{|\alpha|^2}^2 = \overline{K}^2\ \overline{|\alpha|^2}^2. \quad (56)$$

(The last equality in (56) follows from the assumption of independence and equidistribution of the t_k's over $[0, \Delta]$, implying that the t_k point process is Poisson, for which $\overline{K^2} - \overline{K} = \overline{K}^2$.)

With the foregoing assumptions, (51) becomes

$$D = 1 + \frac{\overline{K}}{TW}\cdot\frac{\overline{\mathcal{E}}}{N_0} \quad (57)$$

where $\overline{\mathcal{E}} \triangleq \overline{|\alpha|^2}\mathcal{E}$ is the mean energy per bit arriving per path. Thus the degradation due to multipath-induced interference increases with $\overline{K}\overline{\mathcal{E}}/N_0$ (as this interference from multiple paths increasing dominates the channel noise) and decreases with TW (as the sidelobes of $\gamma(t)$, hence the interference contribution by each interfering path, decrease).

As an example, suppose—using parameters typical of the simulation experiments in Section VI—that $\overline{K} \cong 25$, $TW = 127$ and $\overline{\mathcal{E}}/N_0 = 5$ dB. Then $D = 1.62$, or 2.1 dB, not much degradation to pay for the ability to increase the data rate by, say, a factor of 10 or more by making $T << \Delta$!

We close this section by noting that if the errors in the estimates $\{\hat{a}_k\}$, $\{\hat{\theta}_k\}$, $\{\hat{t}_k\}$ are taken into account, then, as shown in Appendix C, another term having value $\mathcal{E}\Delta/\mathcal{E}_x T$ is added to (57), where $\mathcal{E}_x$ is the sounding signal's energy. By ignoring estimation noise, we have implicitly assumed that $\mathcal{E}_x/\mathcal{E} >> \Delta/T$.

Although the analysis above was performed for a purely coherent PSK system, we shall assume in Section VI that the main results, (51) and (57), carry over approximately to a DPSK system.

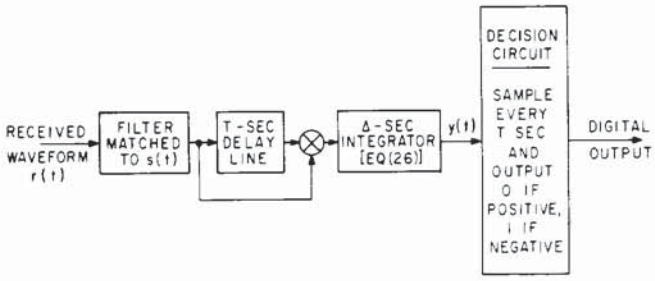

Fig. 21. PDI: A quasi-optimal DPSK receiver for unknown path delays.

V. Simplied Analysis of Error Probability

Exact evaluation of the error probability of a multipath receiver quickly becomes intractable as the assumed model for the multipath channel becomes more realistic. Most analyses assume independent, Rayleigh-distributed path strengths, although some also involve Rice [13] or Nakagami [4] strength distributions and/or correlated strengths [21], [31]. With some exceptions [4], [31], the path strengths are assumed to be equidistributed and the path delays known. None of the cited analyses takes into account the multipath-induced interference discussed in the previous section, although Monsen [15]–[17] and Morgan [18] consider such interference in a different context. Exact analytical evaluation of the error probability for the model in Section II—involving unknown, non-Poisson path delays; correlated Nakagami-distributed path strengths; spatial correlations and inhomogeneities; and multipath-induced interference—seems beyond tractability.

Another approach is to evaluate the error probability of various receivers by simulation techniques, using the channel simulation program described in Section II; the results of a few such simulation experiments are given in Section VI. In the present section, however, we shall present a much simplified analysis. This analysis will provide both intuitive insight into the performance of several receivers, and a basis for determining (in Section VI) the gap between reality and the results of rather standard analytical methods used. In our analysis, we assume lack of knowledge of path delays, but still use very much oversimplified statistics for the path delays and strengths. We temporarily suppress the effects of multipath-induced interference, taking them into account later in Section VI.

We limit ourselves here to a system using DPSK transmission and simplifications of the receivers of Fig. 11 and 17. The analysis depends heavily upon the work of Charash [3], [4].

A. Post-Detection Integrating Receiver

A simplification of the receiver of Fig. 11 is shown in Fig. 21, where the pertinent portion of Fig. 10 is also included. Notice that the (generally time-varying) nonlinearity $\tilde{F}[\cdot, \cdot]$ has been eliminated, i.e., replaced by a time-invariant linear device. For the case of Rayleigh path strengths with equal mean-square values, the nature of the approximation is shown in Fig. 12 (see also (19) and (24)). By eliminating $\tilde{F}$, we are giving up the strong-path-accentuation/noise-suppression features of the receiver that is shown by the waveforms of Fig. 13(c) and (d).

In Fig. 21, we also have taken the integrating filter's impulse response $h_p(t)$ to be of the form of (26). If this $h_p(t)$ were optimal, it would mean that paths occur with uniform density

over the interval $[0,\Delta)$; see Section III-C, where we would have $p(t_k) = 1/\Delta$, $0 \leqslant t_k \leqslant \Delta$. In actuality, paths do not occur uniformly, so this $h_p(t)$ is suboptimal. Since the lowpass filter of Fig. 10 serves only to eliminate the double-carrier-frequency terms in the multiplier output, its function is handled in Fig. 21 by $h_p(t)$, also a lowpass impulse response.

The decision circuit input in Fig. 21 will still look much like the waveform of Fig. 13(e), but it will now be an integration of $y(t)$ of Fig. 13(c), rather than of Fig. 13(d). It must still be sampled by the decision circuit at the instants shown in Fig. 13(f).

The simplified suboptimal receiver just discussed has also been considered by Fralick [7], who descriptively calls it a post-detection integrator (PDI), a name we shall use.

The error-probability performance of the PDI can be estimated from the work of Charash [3], [4]. He has given error-probability expressions and curves for a system having the following characteristics:

1) binary transmission using uniformly orthogonal, zero-sidelobe signals, i.e., ones for which $|\gamma_{12}(t)|$ of (7) is identically zero rather than merely satisfying (8a), and $|\gamma_{ii}(t)|$, $i = 1,2$, is identically zero for $|t| > 1/W$ rather than merely satisfying (8b);
2) a receiver of the form of Fig. 7 (with $M = 2$), but with the nonlinearity being a simple time-invariant square law device, $\hat{F}(x,t) = x^2$;
3) an integrating-filter impulse response, $h_p(t)$, of the form of (26).

Note that this system bears the same relationship to our DPSK/PDI system in the multipath case as the usual orthogonally keyed binary system bears to a standard DPSK system in the single-path case (cf. Figs. 5 and 10). We shall exploit this relationship to estimate the error probability for the DPSK/PDI system.

Charash also makes the following assumptions about the channel:

4) all paths are independently and identically Nakagami-distributed;
5) exactly K paths arrive at random over $[0,\Delta]$. Of course, to preserve resolvability condition 4), we must have $K \ll W\Delta$, where W is the transmission bandwidth;
6) $\Delta \ll T$, so there is no appreciable intersymbol interference;
7) the additive channel noise is white and Gaussian, with single-ended power density N_0.

Under these seven assumptions, Charash has derived an expression for the bit error probability $P_E(K)$ conditioned on the number of paths K. (The unconditional bit error probability would then be the average of $P_E(K)$ over the Poisson distribution of K that is implied by (5).)

As mentioned, our DPSK/DPI system is related to Charash's system in the same way as an ordinary single-path DPSK system is related to an ordinary single-path orthogonally keyed system. The performance of these latter, single-path systems are well known [24] to be exactly 3 dB separated, with the DPSK system having the advantage; i.e., the DPSK system requires 3 dB less SNR to achieve the same bit error probability as the orthogonally keyed system. We now conjecture that the same 3-dB separation holds (at least approximately) for the corresponding multipath systems.

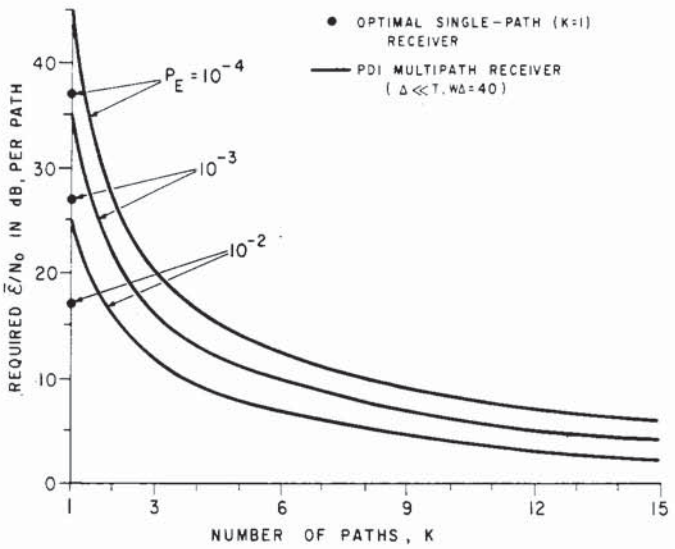

Fig. 22. Required $\bar{\mathcal{E}}/N_0$ per path for DSPK/PDI system: K independent, Rayleigh-fading paths.

Using this conjecture, we have used Charash's results to estimate the error-probability of the DPSK/PDI, of course still assuming that assumptions 3)–7) hold and that the DPSK signal has zero sidelobes. Fig. 22 shows some typical results, for Rayleigh fading (a special case of Nakagami fading) and for $W\Delta = 40$. The curves there show the SNR $\bar{\mathcal{E}}/N_0$ required per path (see (57) *et seq.*) in order to achieve a given value of $P_E(K)$, as a function of the number of paths K. Note that, since typical urban multipath spreads are $\Delta \cong$ 4-5 μs, $W\Delta = 40$ implies a system bandwidth of 8–10 MHz; and since we postulate that $\Delta \ll T$ for the PDI, we are assuming a spectrum spreading factor of $TW \gg 40$.

On the $K = 1$ axis, we have shown for reference the performance of the optimal single-path DPSK receiver of Fig. 10.[20] One can see that if a multipath medium has a number of Rayleigh paths of more-or-less equal mean-square strengths, our DPSK/PDI system will do substantially (5–20 dB) better than a receiver that locks onto a single path, say the LOS path, and disregards the remaining paths. This comparison strikingly illustrates the diversity performance improvement that multipath channels can afford, as discussed at the beginning of Section III.

It must be stressed that the curves of Fig. 22 take into account neither intersymbol interference nor interpath interference (see footnote 11). The former is precluded by the assumption $\Delta \ll T$, the latter by the assumption of a zero-sidelobe signal.

B. A Digital RAKE Receiver

The channel-sounding receivers of Figs. 16 and 17 involve adjustment of the tap gains of the transversal filter(s) with estimates of path strengths. An arrangement that is much simpler to implement, although it will not perform as well, is as follows: connect each tap to the summing bus or not according as it is estimated that a path is present at that delay or not.

[20] This is derived by averaging the nonfading, single-path DPSK error probability [24] of $(1/2)\exp[-\mathcal{E}/N_0]$ over a Rayleigh distribution for $\sqrt{\mathcal{E}}$ having *rms* value $\sqrt{\psi}$, to obtain $P_E = [2(1 + \bar{\mathcal{E}}/N_0)]^{-1}$, where $\bar{\mathcal{E}} = \psi\mathcal{E}$.

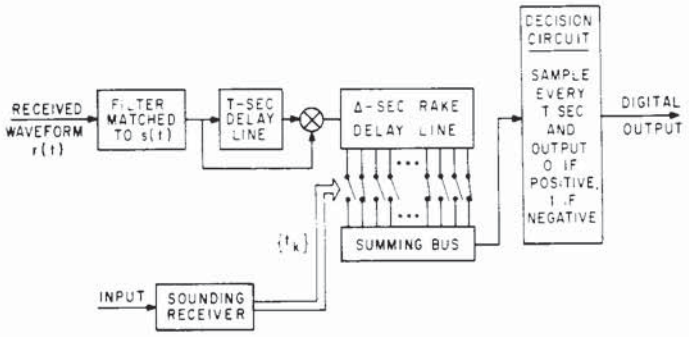

Fig. 23. DRAKE: A quasi-optimal DPSK receiver when path delays are estimated.

Only a transfer of the estimates $\{\hat{t}_k\}$ of the path delays is then needed from the sounding receiver to the transversal filter(s). We call this simplified configuration a digital RAKE (DRAKE) receiver.

Fig. 23 shows a DPSK/DRAKE receiver based on Fig. 17, in which, as a further simplification, the square rooter has been eliminated. The sounding receiver's estimates of path delays turn the associated tap switches on the transversal filter on, connecting the taps to the summing bus. Note that if all tap switches were turned an, Fig. 23 would revert approximately to the PDI of Fig. 21, with the Δ-second integration replaced by an approximating Δ-second discrete-time summation.

In analyzing the DPSK/DRAKE receiver, we assume that the sounding receiver's estimates $\hat{\tau}_k$ of the t_k are exact ($\hat{t}_k = t_k$), and that these estimates correspond exactly to available discrete tap delays in the transversal filter. The receiver then takes the form of an equal-weight path combiner for known path delays. Charash [3], [4] has given expressions and curves for such a receiver under assumptions 1), 4), 5), 6) and 7) of the previous subsection. We can convert these results to the DPSK format of interest to us by the same conjecture as used previously, i.e., that Charash's orthogonally keyed system performs 3 dB worse than our DPSK system. On this basis, curves of the required $\bar{\mathcal{E}}/N_0$ per path necessary to achieve a given P_E are shown in Fig. 24 as functions of the number of paths K. Only curves for the Rayleigh-fading case are shown here; these could also have been obtained from [31].

As in the case of Fig. 22, the curves of Fig. 24 take into account neither intersymbol interference nor the interpath interference in the current symbol. Both of these introduce an effective additional noise term. The performance degradation caused by this term has been estimated in Section IV for an ideal, coherent PSK/RAKE system. In the next section, we shall modify our error-probability analysis by assuming that this same degradation holds approximately for DPSK/DRAKE.

VI. Simulation Experiments

In order to evaluate the error probabilities of various receivers in an actual urban multipath environment and to assess the applicability of the simplied analyses of the previous two sections, a number of simulation experiments were performed. These experiments combined the urban propagation program SURP described in Section III-D and various binary modulator/demodulator programs described below. Two sets of experiments were performed: low rate at 78.7 kb/s and high rate at 787 kb/s. The experiments reported here were restricted to DPSK transmission and to the dense-high-rise environment

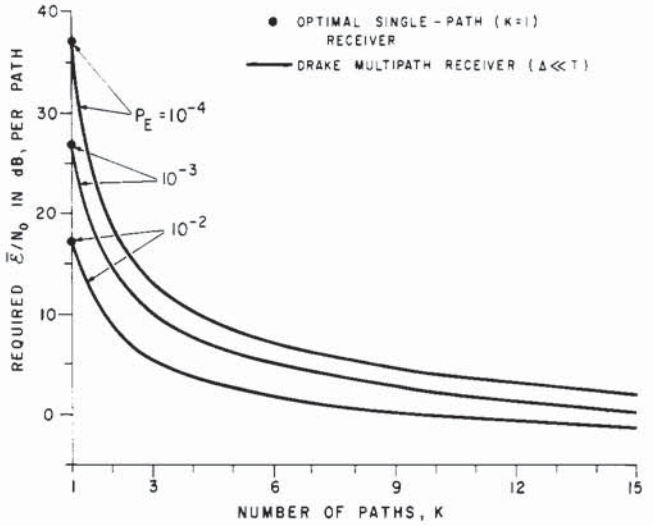

Fig. 24. Required $\bar{\mathcal{E}}/N_0$ per path for DPSK/DRAKE system: K independent, Rayleigh-fading paths.

(Area A); other experiments are in progress, and will be reported in detail elsewhere.[21]

A. Multipath Data Base

As a first step, a data base of urban/suburban multipath profiles were obtained by using SURP.[22] For each of the four areas A, B, C, D, defined in Section III-A, 150 000 profiles were generated along a track 3000-ft long (see Fig. 3), with uniform spacings of 0.02 ft, using L-band (1280 MHz) program parameters. In order to reduce the cost of the runs, new $\{\tau_l\}$ and $\{a_k\}$ strings were generated only at every fifth point, i.e., at 0.1-ft (0.12 wavelength) spacings, and used again for the subsequent four points. (This approximation is quite justified, since spatial correlation distances for $\{\tau_l\}$ and $\{a_k\}$ are tens of wavelengths.) However, since the correlation distance for the $\{\theta_k\}$ string is a fraction of a wavelength, a new $\{\theta_k\}$ string was generated at every point.

Some typical $\{\tau_l\}$ strings and a_k and θ_k values are shown in Fig. 25. One see the $\{\tau_l\}$ strings beginning to decorrelate after about one wavelength and showing substantial decorrelation after 10 wavelengths. Bin 13 happens to have a path in all $\{\tau_l\}$ strings shown, and the corresponding a_k and θ_k values generated for that bin are displayed. Again, for a_k, one sees partial decorrelation at one wavelength and substantial decorrelation after 10 wavelengths. On the other hand θ_k begins to decorrelate at 0.1 wavelength and shows substantial decorrelation at 1 wavelength.

The generated profiles were stored on tape. In addition, for future use in planned narrow-band experiments, the phasor sums $\Sigma_k\, a_k{}^{(n)} \exp\,[j\theta_k{}^{(n)})] = A_n \exp\,(j\psi_n)$ were computed and stored for each $n (n = 1, \cdots, 150\,000)$.

B. Low-Rate Experiments

Recall from Fig. 2 that the simulated multipath profiles are discrete-time impulse responses of a low-pass equivalent chan-

[21] The communication system simulation programs were written and run by M. Kamil. They are part of a Ph.D. thesis in progress, the aim of which is to explore urban mobile digital systems by simulation, in much more depth than the results given here.

[22] This data base was established by H. Hashemi.

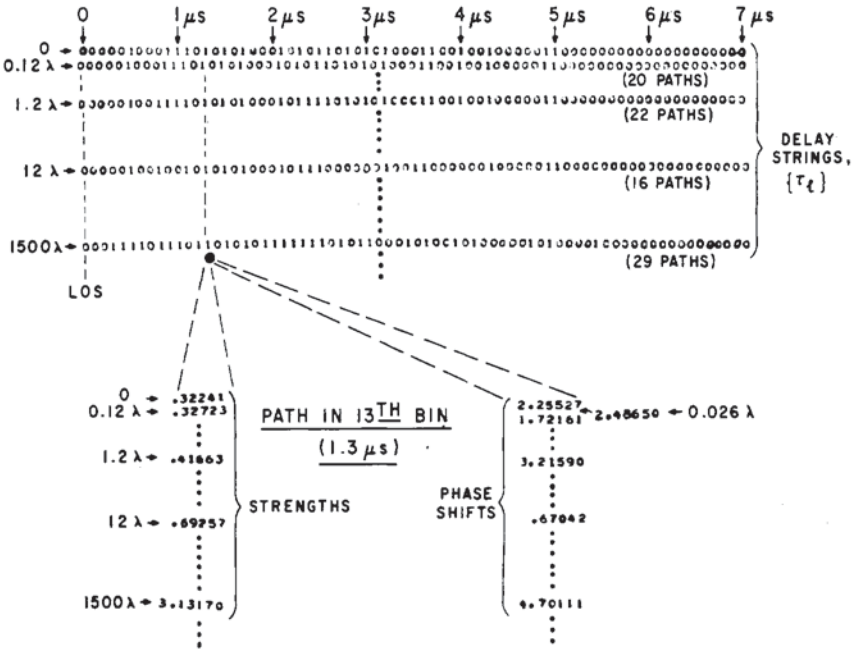

Fig. 25. Typical $\{\tau_l\}$ strings and a_k and θ_k values generated for L-band, using SURP.

nel filter, with time running in 100-ns increments. In designing the "low-rate" communication system simulation experiments, we postulated a DPSK transmitted signal whose basic low-pass-equivalent waveform $s(t)$ is a 127-chip maximal-length shift register (MLSR) sequence having a 100-ns chip duration.[23] Denoting the chip sequence by $\{s_j\}_0^{126}$, the low-pass-equivalent transmitted signal for an N-bit transmission is then of the form

$$w_i = \sum_{n=0}^{N} d_n s_{i-127n}, \qquad i = 0, \cdots, 127N - 1. \quad (58)$$

Here, s_j is defined to be zero for j outside [0,126], and $d_n d_{n-1} = \pm 1$ according as bit $n (n = 1, \cdots, N)$ is 0 or 1, respectively (see Fig. 13(a), (b)).

The w_i sequence was convolved with a space-varying sequence of multipath profiles to form a channel output sequence that simulated the effect of vehicle motion. To this were added independent complex-valued Gaussian noise samples having variance σ_n^2, which was made a program parameter to allow adjustment of the SNR. The noisy received sequence was then convolved with the matched filter impulse response $\{s_{126-i}\}_{i=0}^{126}$.[24]

At this stage, one has a discrete-time representation of the matched-filter output in Fig. 21 or Fig. 23. This output was then DPSK demodulated by multiplying it by the complex-conjugate of a 127-chip-delayed version of the same output and taking the real part of the product. No nonlinear enhancement (e.g., as in Fig. 11) was attempted. The DPSK-demodulator output, which is a noisy discrete-time version of Fig. 13(c), was processed directly by various decision mechanisms, to be described.

The signal format we are using in this low-rate case implies the following parameters: signal bandwidth, $W = (100\text{ ns})^{-1} = 10$ MHz; spectrum spread factor, $TW = 127$; bit rate, $1/T = 78.7$ kb/s. Further, since the multipath profiles are restricted to 71 samples spaced by 100 ns (see Fig. 2), we have $W\Delta = 70$. Thus $\Delta/T = 0.55$, so that intersymbol interference is negligible.

Notice that a vehicle moving even at 60 mph will move only about 0.001 ft (about 10^{-3} wavelength at L-band) per bit, so bit-to-bit changes in the phases $\{\theta_k\}$ negligibly affect the DPSK demodulation. We therefore simplified the experiments by "sampling" the transmissions periodically in space. That is, we imagined that the vehicle listened to 10 bits at each of 10 000 spatial positions spaced 0.3 ft (0.39 wavelength) apart, for a total of 100 000 bits per experiment. In this way, we obtained adequate data to determine bit error probabilities down to $10^{-4} - 10^{-5}$, while guaranteeing a representative geographical cross section (3000 ft) of multipath responses and a representative ensemble of noise waveforms.

Seven decision mechanisms, operating on the simulated DPSK demodulator output, were evaluated. These are described below, and should be visualized in connection with the waveform $y(t)$ in Fig. 13(c).

1) First Path (FP): This is a classical mechanism, in which, in each bit interval, the first threshold crossing of $|y(t)|$ is examined, and a 0 or 1 is decided according as $y(t)$ is positive or negative. In our experiment, the threshold level on $|y(t)|$ was set so that it would be exceeded if the corresponding peak in the matched-filter output exceeded the *rms* value of the noise in the output. For simplicity in running the simulations, we idealized the mechanism by assuming that the first threshold crossing was always due to a signal peak. The position of the first signal-peak crossing was artificially estimated by having the program successively compare the noiseless path strengths

[23] The use of an MLSR sequence has a beneficial effect in our context: whenever $s(t)$ is sent twice with the same polarity, the right-hand sidelobe fluctuations of the matched filter's first response cancel the left-hand sidelobe fluctuations of the second response, thus considerably reducing interpath and intersymbol interference. This cancellation is a well-known property of MLSR sequences [29].

[24] In fact, for computational convenience, the order of the operations was quite different: the convolution of $\{s_i\}$ with $\{s_{126-i}\}$ was done first, then the modulation with the d_n sequence, then the convolution with the multipath profile, then the addition of appropriate noise.

$a_0, a_1, a_2, \cdots$ (which are known to the computer, but not to the receiver) with a threshold related to that set on $|y(t)|$. Because of this idealization, we expect our simulation result to be a lower bound on the error probability of the actual mechanism.

2) Largest Path (LP): Here, the largest peak in $|y(t)|$ in each bit interval is examined and the polarity of this peak determines the output. Again we idealized (not much of an idealization in this case) by assuming that the largest peak is a signal peak. Its position was identified as that of the largest a_k.

3) Post-Detection Integrator (PDI): This is the decision mechanism of Fig. 21. However, instead of integrating over a full $\Delta = 7$-μs interval, we integrated only over a 4-μs interval beyond the LOS path.

4) Adaptive Post-Detection Integrator (APDI): Here, the PDI integrator was made adaptive by letting the integration interval run only from the first crossing to the last crossing of $|y(t)|$ above a threshold. The threshold level and the method of determining the first and last crossing positions were identical to those used for the FP mechanism.

5) Weighted Post-Detector Integrator (WPDI): Recognizing that later paths in a multipath profile are likely to be weaker and less frequent than earlier paths, we here changed the impulse response of the integrator of Fig. 21 from the boxcar $h_p(t)$ of (26) to one with exponential weighting: $h_p(t) = \exp[-(\Delta - t)/\tau]$, $0 \leqslant t \leqslant \Delta$, where the time constant τ was set at 1.5 μs.

6) DRAKE: This is the receiver of Fig. 23. The switch positions were determined by assuming that the sounding receiver will identify as paths only those that are strong enough to cause $|y(t)|$ in the data receiver to exceed a threshold. The threshold level and the method for identifying above-threshold paths are as in the FP mechanism.

7) RAKE: Here, Fig. 23 is modified to restore the ideal tap amplifiers of Fig. 14 in place of the switches. The amplifier gains were determined by assuming that the sounding receiver's estimates of the a_k's are perfect. (See Appendix C.)

Mechanisms (1), (4), and (6) depend on there being at least one path above threshold. At very small SNR's, there were a small number of multipath profiles for which no path exceeded the threshold, and the demodulators deleted the corresponding sequence of 10 bits. Since these bits by definition are very noisy, ignoring them leads to an optimistic estimate of the error probability P_E. The effect was not serious, however, causing less than a 10 percent bias for $P_E \gtrsim 0.1$ and no noticeable bias for $P_E \lesssim 0.1$. But, in order to assure valid comparison of mechanisms (1), (4), and (6) with (2), (3), (5), and (7), which have no threshold but which would be adversely affected by inclusion of the noisy bits, we deleted these bits from the latter demodulator outputs also.

The empirical bit error probability curves determined from the simulation are shown in Fig. 26 as functions of both $\bar{\mathcal{E}}_{av}/N_0$ and $\bar{\mathcal{E}}_{LOS}/N_0$. Here, N_0 is the (single-ended) channel noise power density, as defined in Section IV. $\bar{\mathcal{E}}_{av}$ is the average energy received per bit per path, determined by calculating the mean-square path strength of all paths in all profiles used in the experiment. $\bar{\mathcal{E}}_{LOS}$ is the average energy received per bit on only LOS paths, determined by calculating the mean-square LOS path strength in all profiles having an LOS path. In actual system design, $\bar{\mathcal{E}}_{LOS}$ is a quantity derivable from the power budget, being determined from free-space and excess-attenuation calculations [33].

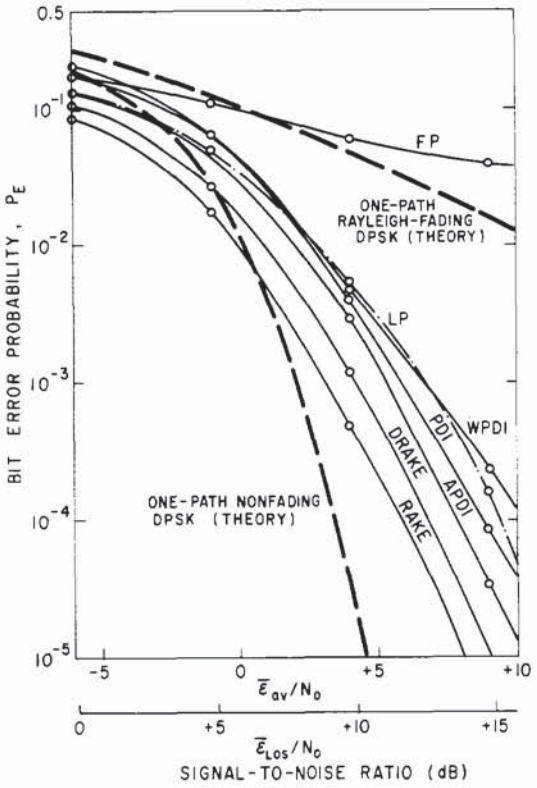

Fig. 26. Error probabilities for the low-rate case, from simulations; dense-high-rise topography ($TW = 127$, $\Delta/T = 0.55$, $R = 1/T = 78.7$ kb/s).

For comparison, also shown in Fig. 26 are classical error-probability curves for an optimal DPSK system operating through a single-path channel, either nonfading or Rayleigh fading (see footnote 20). For these curves, the abscissa is $\bar{\mathcal{E}}_{LOS}/N_0$, where $\bar{\mathcal{E}}_{LOS}$ is the average energy received per bit over the single path, the $\bar{\mathcal{E}}_{av}/N_0$ scale has no meaning for the comparison curves.

From Fig. 26, we can draw the following conclusions.

1) Comparison of the theoretical one-path Rayleigh-fading curve with the empirical first-path-above-threshold (FP) curve shows that path fading (at least of initial paths) is worse than Rayleigh, a conclusion already drawn by Suzuki [26] and Charash [4]. (The fact that the FP curve lies below the Rayleigh curve for small SNR merely shows the value of searching for an above-threshold path when the noise is substantial, rather than always utilizing the same path.) Comparing of the FP curve with Charash's single-path P_E curves [4], as appropriately modified for DPSK signalling, shows that the FP curve reflects Nakagami fading with parameter $m = 0.75$, rather than $m = 1$ (Rayleigh fading).

2) Comparison of the WPDI and PDI shows that a 4-μs boxcar integrator outperforms a 1.5-μs exponentially weighted integrator, at least for dense urban multipath. However, there is reason to believe that for other urban areas and for other time constants, this conclusion might be reversed.

3) An LP receiver, which "captures" the largest peak in $y(t)$, works overwhelmingly better than one that captures the first available peak. (This is the familiar "largest of" voting diversity effect.) In fact, the FP receiver works less than one dB worse than a PDI in the range $10^{-5} \leqslant P_E \leqslant 10^{-2}$, provided that the largest peak in $y(t)$ indeed corresponds to the largest path rather than to noise. However, we note that the PDI is

easier to implement than the FP receiver, among other things requiring less-accurate sampling and timing circuitry.

4) Progressing through successively more complex systems (PDI, APDI, DRAKE, and RAKE) gains of the order of 1 dB per step, provided that APDI, DRAKE, and RAKE have perfect estimates of the path information they need. It is this moderate gain in performance as one progresses through a sequence of substantially more and more sophisticated receivers that supports our faith in their quasi-optimality, as discussed in Section III-G. Changing from PDI (unknown delays) to DRAKE (known delays) results in only a 2-dB improvement, whence it seems certain that PDI is a very close to optimal for unknown delays. Again, changing from DRAKE (unknown strengths, known delays) to RAKE (known strengths, known delays) yields only 1 dB, whence it would seem that DRAKE is close to optimal for a delay-only channel-estimating receiver and RAKE is close to optimal for a delay-and-strength estimating receiver.

5) Because of their path-combining characteristics, by which they accumulate the energies of many almost-independent paths, the WPDI, PDI, APDI, DRAKE, and RAKE receivers operate at an enormous advantage over a receiver that utilizes only a fixed single fading path. At small SNR, they even moderately outperform a receiver that utilizes a single *nonfading* path;[25] while they lose this moderate advantage at large SNR, their performance still comes within a few decibels of the nonfading single-path case. (See Monsen [15] for a similar result obtained by equalization techniques.)

If equipment simplicity is taken into account as well as performance, it would seem desirable to choose the PDI receiver in this low-rate case, for at the expense of less than 2 or 3 dB in SNR the PDI can be substituted for the vastly more complicated DRAKE or RAKE. APDI, while relatively simple, outperforms PDI by less than 1 dB, scarcely worth the additional threshold, AGC and integrate-and-dump features of APDI.

As we have seen, however, the PDI structure is quite susceptible to intersymbol interference. Thus in the high-rate case ($\Delta >> T$), we must rely on RAKE and DRAKE, with all their complexities. We investigate the high-rate performance of RAKE and DRAKE in the following section.

C. High-Rate Experiments

In the high-rate experiments, we increased the data rate by a factor of 10, i.e., to $1/T = 787$ kb/s. Since Δ remains at 7 μs, we now have $\Delta/T = 5.5$, so considerable intersymbol interference exists: 6 predecessor and 6 successor symbols affect the present symbol.

We wish to maintain the same spectrum spreading factor, $TW = 127$, which means that W is now 100 MHz.[26] A problem is posed by this increased bandwidth, for it implies a resolution of $1/W = 10$ ns in the multipath model, while our fundamental data and channel simulation program are based on 100-ns resolution. Unfortunately, virtually no 10-ns-resolution data on the urban channel at the frequencies under consideration are available. (See [10], however.)

We have resolved this dilemma by an approximate extrapolation of our 100-ns data. Each 100-ns bin in Fig. 2(a) was divided into 10 subbins. If $\tau_l = 1$ for some $l \neq 0$, the corresponding path was placed at random in one of the 10 subbins; and if $\tau_0 = 1$, i.e., an LOS path exists, the path was always placed in the first subbin. Thus implicitly, we have structured the multipath to preclude an average of more than one path every 100 ns. While this restriction almost certainly varies from reality, it allows us to use SURP and the data base generated by it for the high-rate case. Hopefully, the resulting simulation results will not be too far off.[27]

In other respects, the high-rate experiment followed the low-rate experiment. DPSK signaling was postulated, using the same MLSR sequence, but now having a 10-ns chip duration and a 1.27-μs bit duration. The multipath impulse response with which the transmitted signal (58) is convolved is now 710 samples long rather than 71, but consists of more than 90 percent zeros. Only RAKE and DRAKE were evaluated, for, as seen in Sections III-F and IV, only they are capable of suppressing intersymbol interference. (WPDI, PDI, and APDI irretrievably scramble the responses to different symbols, while FP and LP present substantial difficulties in deciding which is the first or largest path of the current symbol amidst the interlaced responses to several symbols.)

The results of the high-rate experiment, again run for approximately 100 000 bits per point, are shown in Fig. 27, where the RAKE and DRAKE low-rate results are also shown for comparison.

We see that, as predicted in Section IV, the presence of substantial intersymbol interference does not drastically curtail system operation. In fact, the degradation formula (57), although derived for coherent RAKE and a much simplified multipath model, proves to be remarkably accurate. The average number of paths per profile encountered in the simulation run was 23.2. If we allow the simplified multipath model of Section IV to have $\overline{K} = 23.2$ paths and the $\overline{\mathcal{E}}/N_0$ parameter of that model to be identified with $\overline{\mathcal{E}}_{av}/N_0$ of Fig. 27, then, setting $TW = 127$, D of (57) is 1.3 dB at $\overline{\mathcal{E}}_{av}/N_0 = 3$ dB, 2.0 dB at $\overline{\mathcal{E}}_{av}/N_0 = 5$ dB and 2.8 dB at $\overline{\mathcal{E}}_{av}/N_0 = 7$ dB. These are almost exactly the gaps between the two RAKE curves shown in Fig. 27.

Again we see that changing from DRAKE to RAKE yields only a modest improvement (2–3 dB), and we therefore guess that the optimal receiver will not substantially outperform RAKE.

D. Comparison with the Simplified Theory

In Section V, we gave theoretical error-probability curves for the low-rate PDI and DRAKE demodulators; see Figs. 22 and 24. Since these curves were based on a number of very simple but often-used assumptions (uniformly distributed Poisson path arrivals; independent Rayleigh-distributed path strengths; no intersymbol interference; a zero-sidelobe DPSK

[25] Much of this small-SNR advantage over nonfading, single-path operation is real, reflecting the benefits of path combination when the noise is large. Some of the advantage, however, reflects the previously mentioned bias in the experiment at small SNR due to discarding certain "bad" profiles.

[26] This large bandwidth does not require exclusive assignment, however, as many systems with different codes could coexist in the same band; see [40] for a discussion of a spread-spectrum code-multiplexed digital-voice system proposed for urban use.

[27] Since we are dealing with an average of about 25 paths per profile, it is unlikely that use of a refined 10-ns model—having, say, 50–75 paths per profile but delivering the same total energy—would result in a substantially different error rate. This assertion follows from the well-known phenomenon that most diversity gain accrues from the addition of only a few diversity links, the point of diminishing returns being quickly reached.

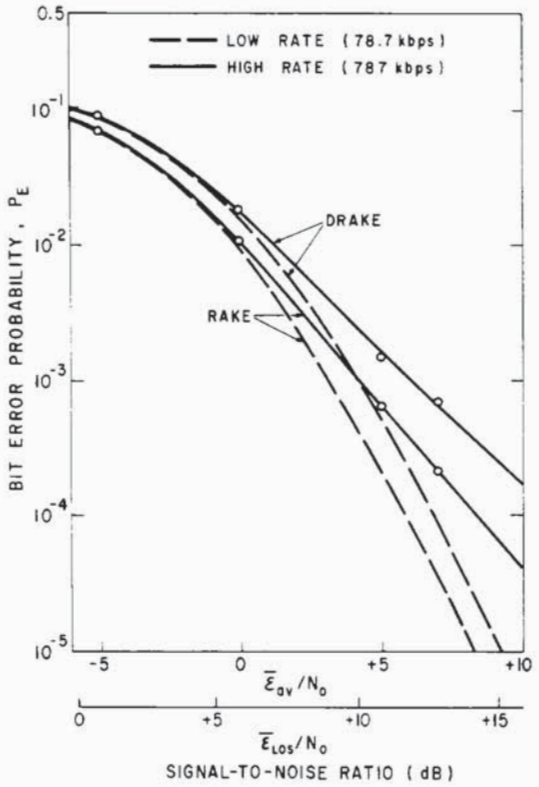

Fig. 27. Error probabilities for the high-rate case, from simulations; dense high-rise topography ($TW = 127$, $\Delta/T = 5.5$, $R = 1/T = 787$ kb/s).

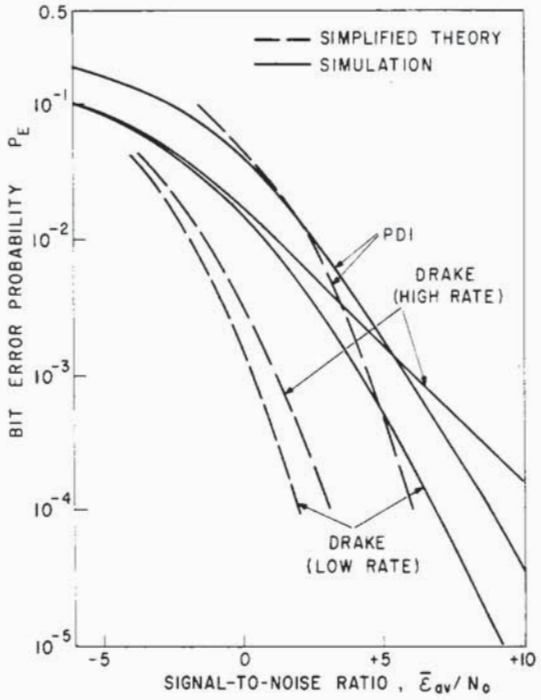

Fig. 28. Comparison of simplified theory with experiment.

signal, i.e., no interpath interference), it is of value to compare them with reality. The comparison is shown in Fig. 28. There, we have redrawn the simulation-derived low-rate PDI and DRAKE curves from Fig. 26 and the high-rate DRAKE curve from Fig. 27. Also shown are theoretical low-rate PDI and DRAKE curves taken from Figs. 22 and 24 (as extended from [3]), which were obtained by extrapolating Figs. 22 and 24 to a value of K equal to the *average* number of paths per profile (23.7) encountered in the simulation. The theoretical high-rate DRAKE curve was obtained from the corresponding low-rate curve by assuming that the degradation given by (57), derived for ideal coherent RAKE, applies approximately also to DRAKE; in (57), we used $\bar{K} = 23.7$.

We see that the simplified theory leads to results that are between 3 and 7 dB optimistic in neighborhood of $P_E = 10^{-4}$, and less so at larger error probabilities. This optimism is due to the combined effects of the following factors.

1) As we have noted in connection with the FP curves of Fig. 26, actual urban fading is worse than Rayleigh. Reference to the worse-than-Rayleigh curves of [3] show that the Rayleigh assumption leads to about 1-dB worth of optimism at $P_E = 10^{-4}$.

2) Actual urban paths are correlated, rather than independent; we estimate that assuming independence leads to another 1 dB of optimism.

3) Because of spatial inhomogeneities, actual path strengths have variances that are smaller in local areas than on a global basis. The simplified theory imagines that the global variances apply at each local site, leading to a larger-than-actual "path diversity" gain.

4) The actual DPSK signal used did not have zero sidelobes, so more interpath and intersymbol interference exists than in the simplified theory. We estimate from Section IV that ignoring this interference accounts for about 2.5 dB of optimism at $P_E = 10^{-4}$.

5) Finally, since the theoretical low-rate DRAKE curve is optimistic in estimating the required $\bar{\mathcal{E}}_{av}/N_0$ for a given P_E, use of (57) will lead to an optimistic value of D to be applied in obtaining the high-rate curve, thus compounding the error. The error is further compounded by the assumption that (57) applies to DRAKE, since Fig. 27 shows that the intersymbol interference is more damaging to DRAKE than to RAKE.

Thus the simplified theory, although based on common analytical assumptions, must be treated with caution, especially at $P_E < 10^{-2}$; that is, its optimism should be recognized in attempting to apply it to urban multipath.

Appendix A: Derivation of (46)

From (42) and using the assumptions listed just prior to that equation, we obtain

$$E[|v(0)|^2]|_{d_0=+1} = \sum_{n=-N}^{N} E_K \sum_{k,l,q,r=0}^{K-1} \overline{\alpha_k \alpha_l^* \alpha_q^* \alpha_r} \cdot \overline{\gamma(nT - t_k + t_l)\, \gamma^*(nT - t_q + t_r)} \quad \text{(A-1)}$$

where the overbars denote expectation and E_K denotes expectation over the random variable K. Note that, of all the combinations of the indices k, l, q and r in (A-1), in any instance where one is distinct from the others, the expectation $\overline{\alpha_k \alpha_l^* \alpha_q^* \alpha_r}$ will factor into the form $\overline{\alpha_k \alpha_l^* \alpha_q^*}\ \overline{\alpha_r}$ (where here r is the distinct index); this factorization follows by virtue of the independence of the α_k's. But, because of the assumed uniform distribution of the θ_k's and the independence of the a_k's and θ_k's, $\bar{\alpha}_k = E[a_k \exp(j\theta_k)] = 0$. Thus the only surviving terms in (A-1) are those in which indices are pairwise

equal, and, of these, those where $k = r$ and $l = q$ vanish because $\alpha_k^2 = E[\alpha_k^2 \exp(j2\theta_k)] = 0$. Therefore,

$$E[|v(0)|^2] = \sum_{n=-N}^{N} E_K\Bigg[\sum_{k=0}^{K-1} \overline{|\alpha_k|^4}\, |\gamma(nT)|^2 + \sum_{\substack{k=0 \\ k\neq l}}^{K-1}\sum_{l=0}^{K-1} \overline{|\alpha_k|^2}\,\overline{|\alpha_l|^2}\, |\gamma(nT)|^2 + \sum_{\substack{k=0 \\ k\neq l}}^{K-1}\sum_{l=0}^{K-1} \overline{|\alpha_k|^2}\,\overline{|\alpha_l|^2}\, |\gamma(nT - t_k + t_l)|^2\Bigg] \tag{A-2}$$

where we have noted that (A-1) is independent of d_0.

Since

$$\gamma(t) = \int_{-\infty}^{\infty} |S(f)|^2 \exp(j2\pi ft)\, df \tag{A-3}$$

we have

$$\overline{|\gamma(nT - t_k + t_l)|^2} = \int_{-\infty}^{\infty} |S(f)|^2\, |S(\nu)|^2 \exp[j2\pi(f-\nu)nT] \cdot \overline{\exp[j2\pi(f-\nu)t_k]} \cdot \overline{\exp[-j2\pi(f-\nu)t_l]}\, df\, d\nu. \tag{A-4}$$

If we define $p(t_k)$ to be the probability density distribution of the t_k's, then

$$\overline{\exp(j2\pi ft_k)} = \int_0^{\Delta} p(t_k) \exp(j2\pi ft_k)\, dt_k = P(f) \tag{A-5}$$

is the characteristic function of $p(t_k)$.

We note from (23) *et seq.*, that $|\gamma(nT)|^2 = 0$ for $n \neq 0$. Using this fact and (A-4) and (A-5), (A-2) becomes

$$E[|v(0)|^2] = (2\mathcal{E})^2 \Bigg[E_K \sum_{k=0}^{K-1} \overline{|\alpha_k|^4} + E_K \sum_{\substack{k=0 \\ k\neq l}}^{K-1}\sum_{l=0}^{K-1} \overline{|\alpha_k|^2}\,\overline{|\alpha_l|^2}\Bigg] + \sum_{n=-N}^{N} E_K \sum_{k=0}^{K-1}\sum_{l=0}^{K-1} \overline{|\alpha_k|^2}\,\overline{|\alpha_l|^2} \cdot \iint_{-\infty}^{\infty} |S(f)|^2\, |S(\nu)|^2\, |P(f-\nu)|^2 \cdot \exp[j2\pi(f-\nu)nT]\, df\, d\nu \tag{A-6}$$

where we have used the fact that $\gamma(0) = 2\mathcal{E}$, $\mathcal{E}$ being the energy of the transmitted signal $s(t) = \mathrm{Re}[\sigma(t)\exp(j\omega t)]$.

From (A-5) we see that for a reasonably diffuse $p(t_k)$, in the sense of Section III-C, the "width" of $P(f)$ must be of the order of $1/\Delta$. On the other hand, the width of $|S(f)|^2$ is of the order of W. But we are assuming $TW \gg 1$ and $\Delta > T$, so $W \gg 1/\Delta$. The situation is depicted in Fig. 29, where the factors $|S(f)|^2$ and $|P(f-\nu)|^2$ in the integrand of (A-6) are

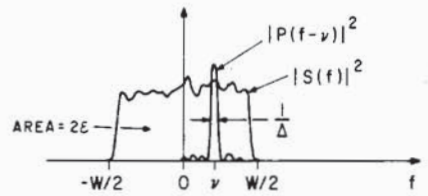

Fig. 29. Illustrating the integration in equation (A-6).

shown. If we assume that $|S(f)|^2$ is smoothly varying, the integral on f in (A-6) can be written approximately as

$$\int_{-\infty}^{\infty} |S(f)|^2\, |P(f-\nu)|^2 \exp(j2\pi fnT)\, df \cong |S(\nu)|^2 \int_{-\infty}^{\infty} |P(f-\nu)|^2 \exp(j2\pi fnT)\, df \cong \begin{cases} |S(\nu)|^2\, q(nT)\exp(j2\pi\nu nT), & |\nu| \leqslant \dfrac{W}{2} \\ 0, & |\nu| > \dfrac{W}{2} \end{cases} \tag{A-7}$$

where

$$q(t) = \int_{-\infty}^{\infty} |P(f)|^2 \exp(j2\pi ft)\, df = \int_0^{\Delta} p(\tau)\, p(\tau - t)\, d\tau. \tag{A-8}$$

The double integral in (A-6) then becomes

$$q(nT)\int_{-\infty}^{\infty} |S(\nu)|^4\, d\nu \tag{A-9}$$

so (A-6) becomes, after a little manipulation,

$$E[|v(0)|^2] = (2\mathcal{E})^2\, E_K\Bigg[\sum_{k=0}^{K-1} (\overline{|\alpha_k|^4} - \overline{|\alpha_k|^2}^2)\Bigg] + (2\mathcal{E})^2\, E_K\Bigg[\Bigg(\sum_{k=0}^{K-1} \overline{|\alpha_k|^2}\Bigg)^2\Bigg] + \Bigg[\int_{-\infty}^{\infty} |S(\nu)|^4\, d\nu\Bigg]\Bigg[\sum_{n=-N}^{N} q(nT)\Bigg] \cdot E_K \sum_{\substack{k=0 \\ k\neq l}}^{K-1}\sum_{l=0}^{K-1} \overline{|\alpha_k|^2}\,\overline{|\alpha_l|^2}. \tag{A-10}$$

The second line in (A-10) is recognizable as the square of $E[v(0)]$ of (44); subtracting it, we get var $[v(0)]$, as given in (46).

Appendix B: Derivation of the Last Term in (50)

Suppose that the channel noise, $n(t) = \mathrm{Re}[\nu(t)\exp(j2\pi f_0 t)]$, is a bandpass white process having spectral density $N_0/2$ in a band around $\pm f_0$. The low-pass-equivalent noise $\nu(t)$ then has a spectral density $2N_0$ in a band of the same width around

$f = 0$ (see [30]). $\nu(t)$ passes through the receiver's cascade of the matched filter and transversal filter, which has overall transfer function $S^*(f)\,H_{tf}(f)$ (see (35)). Assuming that the transversal filter's taps are exactly set ($\hat{\alpha}_k = \alpha_k$, $\hat{t}_k = t_k$, all k), the noise output of this cascade has spectrum

$$U(f) = 2N_0|S(f)|^2 \left|\sum_{k=0}^{K-1} \alpha_k^* \exp(+j2\pi f t_k)\right|^2$$

$$= 2N_0|S(f)|^2 \sum_{k=0}^{K} \sum_{l=0}^{K-1} \alpha_k^* \alpha_l \exp[j2\pi f(t_k - t_l)]. \quad \text{(B-1)}$$

Using the simplified assumptions on multipath statistics listed in Section IV, we can easily show that the average of $U(f)$ is

$$\bar{U}(f) = 2N_0|S(f)|^2 A^2 \quad \text{(B-2)}$$

where A is as in (45). The variance of the noise at the output of the transversal filter is therefore

$$\int_{-\infty}^{\infty} \bar{U}(f)\,df = 4\mathcal{E}N_0A^2. \quad \text{(B-3)}$$

Appendix C: The Effect of Noisy Path Estimates

In the analysis of Section IV, we assumed that the channel-sounding system was capable of supplying perfect estimates of path variables and that the RAKE receiver was capable of using these exactly. In effect, we therefore assumed that the sounding receiver can supply $h_m(t)$ of (30) or $H_m(f)$ of (34) exactly and RAKE can then configure itself into a filter with transfer function $\hat{H}_{tf}(f) = H_m^*(f)\exp(-j2\pi f\Delta)$ (see (35)). We investigate the implications of these assumptions here.

Estimation of the impulse response of an unknown medium has been investigated in [28], where the optimum sounding signal and optimum estimating receiver are derived. Generally speaking, the optimal signal's energy is distributed in a way depending on the noise spectrum and average channel transmission function, while the optimal receiver uses a filter that is between being inverse to and matched to the optimum signal.

When the simplified channel model of Section IV is assumed, however, the optimal signal distributes its energy uniformly over the transmission band of the system and the optimal receiver is matched to this signal. In lowpass-equivalent form, the sounding receiver's matched-filter output is a noisy, band-limited version of (30), i.e.,

$$\hat{h}_m(t) = \sum_{k=0}^{K-1} a_k \exp(j\theta_k)\frac{\sin \pi W(t - t_k)}{\pi W(t - t_k)} + \xi(t) \quad \text{(C-1)}$$

where $\xi(t)$ is a complex low-pass output noise. In (C-1), the $(\sin x)/x$ pulses have been scaled to have the same areas as the corresponding impulses in (30). Hence, the Fourier transform of the first term of (C-1) agrees with that of (30) within the band $|f| \leqslant W/2$.

We approximate the RAKE transversal filter by assuming that its impulse response is

$$\hat{h}_{tf}(t) = \hat{h}_m^*(\Delta - t)$$

$$= \sum_{k=0}^{K-1} \alpha_k^* \frac{\sin \pi W(\Delta - t - t_k)}{\pi W(\Delta - t - t_k)} + \xi^*(\Delta - t) \quad \text{(C-2)}$$

instead of (33). The first term of (C-2) agrees with (33) in the band $|f| \leqslant W/2$ and therefore will act on RAKE input signals identically as (33); to implement it would require infinitesimally spaced taps on the RAKE delay line, however. The second term of (C-2) comprises the noise in the estimate supplied by the sounding receiver.

The second term in (C-2) is that responsible for the degradation in performance due to a noisy sounding estimate. As mentioned, the optimal sounding signal for our case has a flat spectrum,

$$|X(f)| = \sqrt{2\mathcal{E}_x/W}, \quad |f| \leqslant W/2 \quad \text{(C-3)}$$

where $\mathcal{E}_x$ is the sounding energy. In order to have the scaling of (C-2), the magnitude of the frequency characteristic of the sounding receiver's matched filter must be $\sqrt{W/2\mathcal{E}_x}$ over the band. The noise power density of $\xi(t)$ is thus

$$P_\xi(f) = \begin{cases} N_0W/\mathcal{E}_x, & |f| \leqslant W/2 \\ 0, & |f| > W/2 \end{cases} \quad \text{(C-4)}$$

since, from Appendix B, the low-pass-equivalent channel noise has power density $2N_0$.

Let

$$y(t) = \mathcal{F}^{-1}[H_m(f)|S(f)|^2 \exp(j2\pi fT)]$$

$$= \sum_{k=0}^{K-1} \alpha_k \gamma(t - t_k) \quad \text{(C-5)}$$

be the low-pass equivalent signal output of the data receiver's matched filter, in response to a single-signal transmission, as shifted so that its LOS peak occurs at $t = 0$. The RAKE transversal filter convolves this output with $\hat{h}_{tf}(t)$ to form $w(t)$, the signal component of which is specified by (36) and (38). $w(t)$ also has a component due to noisy estimation of channel parameters, obtained by convolving the $\xi^*(\Delta - t)$ of (C-2) with $y(t)$ of (C-5).[28] This component of $w(t)$ has the form

$$\int_0^\Delta \xi^*(\Delta - t)\,y(t - \tau)\,d\tau \quad \text{(C-6)}$$

which, when shifted to the left by Δ seconds, becomes

$$\int_0^\Delta \xi^*(\tau)\,y(t + \tau)\,d\tau. \quad \text{(C-7)}$$

Equation (C-7) gives the estimation-noise component of $w(t)$ when only a single signal is transmitted. When a sequence of signals is transmitted with PSK modulation, as discussed prior to (39), the estimation-noise component becomes

$$\epsilon(t) \triangleq \int_0^\Delta \xi^*(\tau) \sum_{n=-N}^{N} d_n y(t - nT + \tau)\,d\tau \quad \text{(C-8)}$$

where we have indicated that the responses to only $2N + 1$ symbols are in the RAKE delay line at one time.

At $t = 0$, when the signal component of the RAKE filter output peaks for the present symbol (see (42)), the estimation-noise component is

$$\epsilon(0) = \sum_{n=-N}^{N} d_n \int_0^\Delta \xi^*(\tau)\,y(\tau - nT)\,d\tau. \quad \text{(C-9)}$$

[28] There is also a term in $w(t)$ involving convolution of $\xi(t)$ with the noise in the data receiver's matched-filter output; we neglect this.

This has zero mean, since $\overline{\xi^*(t)} \equiv 0$, and variance

$$E[|\epsilon(0)|^2] = \sum_{n=-N}^{N} \sum_{m=-N}^{N} d_n d_m \iint_0^{\Delta} \overline{\xi^*(\tau)\,\xi(\sigma)\,y(\tau - nT)\,y^*(\sigma - mT)}\, d\tau\, d\sigma. \quad \text{(C-10)}$$

Since $\overline{d_n d_m} = \delta_{mn}$ (independent data symbols), and (from (C-4)) $\overline{\xi^*(\tau)\,\xi(\sigma)} = (N_0 W/\mathcal{E}_x)\,\delta(\tau - \sigma)$, and (from (C-5)),

$$\overline{y(\tau - nT)\,y^*(\sigma - mT)} = E_K \sum_{k=0}^{K-1} \sum_{l=0}^{K-1} \overline{\alpha_k \alpha_l^*}\, \overline{\gamma(\tau - nT - t_k)\,\gamma^*(\sigma - mT - t_l)} \quad \text{(C-11)}$$

and using $\overline{\alpha_k \alpha_l^*} = \overline{|\alpha_k|^2}\,\delta_{kl}$ (from the simplified multipath model of Section IV), we have

$$E[|\epsilon(0)|^2] = \frac{N_0 W}{\mathcal{E}_x} \sum_{n=-N}^{N} \cdot E_K \sum_{k=0}^{K-1} \int_0^{\Delta} \overline{|\alpha_k|^2}\, \overline{|\gamma(\tau - nT - t_k)|^2}\, d\tau. \quad \text{(C-12)}$$

Again using the simplified multipath model of Section IV, in which all t_k's are independent and uniformly distributed over $[0, \Delta]$, we have

$$E[|\epsilon(0)|^2] = \frac{N_0 W A^2}{\mathcal{E}_x \Delta} \sum_{n=-N}^{N} \int_0^{\Delta} \int_0^{\Delta} |\gamma(\tau - nT - t_k)|^2\, d\tau\, dt_k \quad \text{(C-13)}$$

where A^2 is given by (45). Using the transformation $u = \tau - t_k$, $v = \tau + t_k$, whose Jacobian is $\frac{1}{2}$, equation (C-13) becomes

$$E[|\epsilon(0)|^2] = \frac{N_0 W A^2}{2\mathcal{E}_x \Delta} \sum_{n=-N}^{N} \int_{-\Delta}^{\Delta} du \int_{|u|}^{2\Delta - |u|} dv\, |\gamma(u - nT)|^2 = \frac{N_0 W A^2}{\mathcal{E}_x \Delta} \sum_{n=-N}^{N} \int_{-\Delta}^{\Delta} (\Delta - |u|)\, |\gamma(u - nT)|^2\, du. \quad \text{(C-14)}$$

Finally, we note that $|\gamma(t)|$ is a narrow pulse of width $1/W \ll \Delta$. Treating it as a delta function of area

$$\int_{-\infty}^{\infty} |\gamma(t)|^2\, dt = \int_{-\infty}^{\infty} |S(f)|^4\, df \quad \text{(C-15)}$$

(since the Fourier transform of $\gamma(t)$ is $|S(f)|^2$, the signal's low-pass-equivalent energy density spectrum), and using (53), we have

$$E[|\epsilon(0)|^2] \cong \frac{4N_0 \mathcal{E}^2 A^2}{\mathcal{E}_x \Delta} \sum_{n=-N}^{N} (\Delta - |n|\,T). \quad \text{(C-16)}$$

When $T > \Delta$, so only the $n = 0$ term exists, equation (C-16) becomes

$$E[|\epsilon(0)|^2] \cong \frac{4N_0 \mathcal{E}^2 A^2}{\mathcal{E}_x}. \quad \text{(C-17)}$$

More interestingly, when $\Delta >> T$, so we can approximate the sum in (C-16) with an integral of value Δ^2/T, we have

$$E[|\epsilon(0)|^2] \cong \frac{N_0 \mathcal{E}^2 A^2}{\mathcal{E}_x} \cdot \frac{\Delta}{T}. \quad \text{(C-18)}$$

$E[|\epsilon(0)|^2]$ is another term to be added to (50), adding to the degradation caused by multipath-induced interference and channel noise. Taking this term into account, the increase in the RAKE output noise variance, as given by (57), now becomes

$$D \cong 1 + \frac{\overline{K}}{TW} \frac{\overline{\mathcal{E}}}{N_0} + \frac{\mathcal{E}}{\mathcal{E}_x} \frac{\Delta}{T} \quad \text{(C-19)}$$

where we have assumed that $\Delta >> T$ and used (C-18).

We thus conclude that if the ratio of sounding-signal energy to data-signal energy satisfies

$$\frac{\mathcal{E}_x}{\mathcal{E}} >> \frac{\Delta}{T} >> 1 \quad \text{(C-20)}$$

then the estimation-noise contribution to the total RAKE output noise is negligible. If, as in the high-rate case of Section VI-C, $\Delta/T = 5.5$, then $\mathcal{E}_x$ should be 10 times or more greater than $\mathcal{E}$ for (C-20) to hold.

Acknowledgment

A heavy debt of gratitude is due the National Science Foundation for its support of underlying basic research on multipath channel characterization and simulation at the University of California (Berkeley). Analyses and simulations of particular systems were supported by the Advanced Research Projects Agency (ARPA) through SRI International. Finally, the author acknowledges with pleasure his students U. Charash, H. Hashemi, M. Kamil, and H. Suzuki, upon whose Ph.D. research this paper heavily relies.

References

[1] P. A. Bello, "Characterization of randomly time-variant linear channels," *IEEE Trans. Commun. Syst.*, vol. CS-11, pp. 360–393, Dec. 1963.
[2] D. G. Brennan, "On the maximum signal-to-noise ratio realizable from several noisy signals," *Proc. IRE*, vol. 43, p. 1530, Oct. 1955.
[3] U. Charash, "A study of multipath reception with unknown delays," Ph.D. Thesis, Dep. Elec. Eng. Comput. Sci., Univ. California, Berkeley, Jan. 1974.
[4] —, "Reception through Nakagami-fading multipath channels with random delays," *IEEE Trans. Commun.*, vol. COM-27, pp. 657–670, Apr. 1979.
[5] D. C. Cox, "A measured delay-doppler scattering function for multipath propagation at 910 MHz in an urban mobile environment," *Proc. IEEE*, vol. 61, pp. 479–480, Apr. 1973.
[6] R. C. Dixon, Ed., *Spread-Spectrum Techniques.* New York: IEEE Press, 1976.
[7] S. C. Fralick, "An improved packet radio demodulator for mobile operation," Temporary packet radio note 132, Stanford Res. Inst., Menlo Park, CA, Mar. 1975.
[8] H. Hashemi, "Simulation of the urban radio propagation channel," Ph.D. thesis, Dep. Elec. Eng. Comput. Sci., Univ. California, Berkeley, Aug. 1977.
[9] —, "Simulation of the urban radio propagation channel," *IEEE Trans. Veh. Technol.*, vol. VT-28, pp. 213–224, Aug. 1979.
[10] R. W. Hubbard *et al.*, "Measuring characteristics of microwave mobile channels," Nat. Telecommun. and Inform. Admin., Boulder, CO, Rep. 78-5, June 1978.
[11] W. C. Jakes, Jr., Ed., *Microwave Mobile Communications.* New York: Wiley, 1974.
[12] R. S. Kennedy, *Fading Dispersive Communication Channels.* New York: Wiley, 1969.
[13] W. C. Lindsey, "Error probability for incoherent diversity reception," *IEEE Trans. Inform. Theory*, vol. IT-11, pp. 491–499, Oct. 1965.
[14] R. W. Lucky *et al.*, *Principles of Data Communication.* New

York: McGraw-Hill, 1968.
[15] P. Monsen, "Feedback equalization for fading dispersive channels," *IEEE Trans. Inform. Theory*, vol. IT-17, pp. 56–64, Jan. 1971.
[16] ——, "Digital transmission performance on fading dispersive diversity channels," *IEEE Trans. Commun.*, vol. COM-21, pp. 33–39, Jan. 1973.
[17] ——, "Adaptive equalization of the slow fading channel," *IEEE Trans. Commun.*, vol. COM-22, pp. 1064–1075, Aug. 1974.
[18] D. R. Morgan, "Adaptive multipath cancellation for digital data communications," *IEEE Trans. Commun.*, vol. COM-26, pp. 1380–1390, Sept. 1978.
[19] D. L. Nielson, "Microwave propagation and noise measurements for mobile digital radio application," Packet radio note 4, Stanford Res. Inst., Menlo Park, CA, Jan. 1975.
[20] ——, "Microwave propagation measurements for mobile digital radio application," *IEEE Trans. Veh. Technol.*, vol. VT-27, pp. 117–132, Aug. 1978.
[21] J. N. Pierce and S. Stein, "Multiple diversity with nonindependent fading," *Proc. IRE*, vol. 48, pp. 89–104, Jan. 1960.
[22] R. Price, "Optimum detection of random signals in noise with applications to scatter-multipath communication," *IRE Trans. Inform. Theory*, vol. IT-2, pp. 125–135, Dec. 1956.
[23] R. Price and P. E. Green, Jr., "A communication technique for multipath channels," *Proc. IRE*, vol. 46, pp. 555–570, Mar. 1958.
[24] M. Schwartz *et al.*, *Communication Systems and Techniques*. New York: McGraw-Hill, 1966.
[25] H. Suzuki, "A statistical model for urban radio propagation," Ph.D. thesis, Dep. Elec. Eng. Comput. Sci., Univ. of California, Berkeley, Apr. 1975.
[26] ——, "A statistical model for urban radio propagation," *IEEE Trans. Commun.*, vol. COM-25, pp. 673–680, July 1977.
[27] G. L. Turin, "Communication through noisy, random-multipath channels," *IRE Nat. Conv. Rec.*, pt. 4, pp. 154–166, 1956.
[28] ——, "On the estimation in the presence of noise of the impulse response of a random, linear filter," *IRE Trans. Inform. Theory*, vol. IT-3, pp. 5–10, Mar. 1957.
[29] ——, "An introduction to matched filters," *IRE Trans. Inform. Theory*, vol. IT-6, pp. 311–329, June 1960.
[30] ——, "On optimal diversity reception," *IRE Trans. Inform. Theory*, vol. IT-7, pp. 154–166, July 1961.
[31] ——, "On optimal diversity reception, II," *IRE Trans. Commun. Syst.*, vol. CS-10, pp. 22–31, Mar. 1962.
[32] G. L. Turin *et al.*, "Urban vehicle monitoring: Technology, economics and public policy," vol. II: Technical Analysis and Appendices," report prepared under DHUD contract H-1030, Oct. 1970.
[33] G. L. Turin *et al.*, "A statistical model of urban multipath propagation," *IEEE Trans. Veh. Technol.*, vol. VT-21, pp. 1–9, Feb. 1972.
[34] G. L. Turin *et al.*, "Simulation of urban vehicle-monitoring systems," *IEEE Trans. Veh. Technol.*, vol. VT-21, pp. 9–16, Feb. 1972.
[35] G. L. Turin, "Simulation of urban radio propagation and of urban radio communication systems," *Proc. Int. Symp. Antennas and Propagat.*, Sendai, Japan, pp. 543–546, Aug. 1978.
[36] J. M. Wozencraft and I. M. Jacobs, *Principles of Communication Engineering*. New York: Wiley, 1965.
[37] W. R. Young, Jr. and L. Y. Lacy, "Echoes in transmission at 450 megacycles from land-to-car radio units," *Proc. IRE*, vol. 38, pp. 255–258, March 1950.
[38] R. E. Kahn *et al.*, "Advances in packet radio technology," *Proc. IEEE*, vol. 66, pp. 1468–1496, Nov. 1978.
[39] E. N. Skomal, *Man-Made Radio Noise*. New York: Van Nostrand Reinhold, 1978.
[40] G. R. Cooper and R. W. Nettleton, "A spread-spectrum technique for high-capacity mobile communications," *IEEE Trans. Veh. Technol.*, vol. VT-27, pp. 264–275, Nov. 1978.

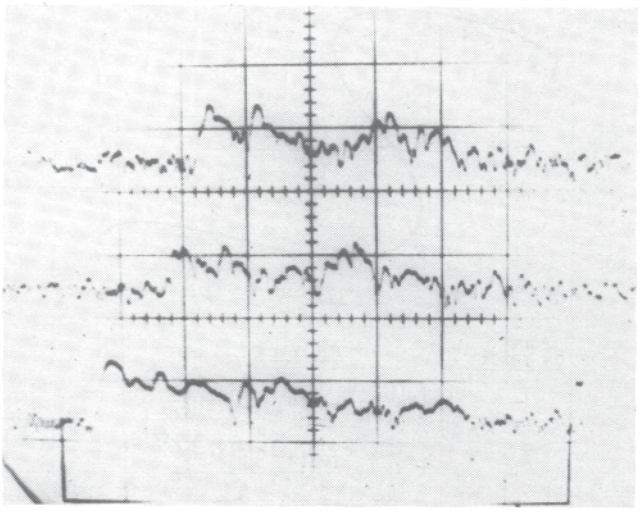

(a)

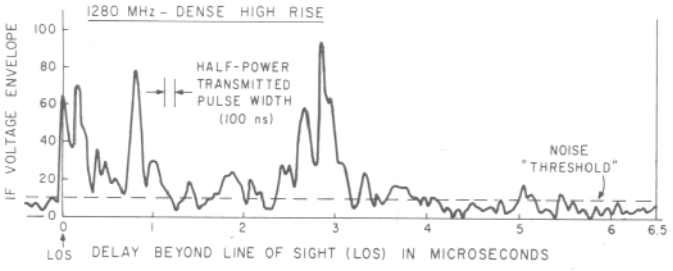

(b)

Fig. 1. Example of measured multipath profiles for a dense high-rise topography. (a) Top to bottom: 2920, 1280, 488 MHz. Vertical scale: 35 dB/cm. Horizontal scale: 1 μs/cm. Different apparent LOS delays are due to difference in equipment delays. (b) Middle trace of (a) on a linear scale.